Pomona College

Undergraduate Thesis

Ultracold Atoms in Line-World: Bose-Einstein Condensates in a Quasi-One Dimensional Gravito-Optical Surface Trap

Author:
Benjamin Girodias

Supervisor:
Dr. Dwight Whitaker

A thesis submitted in fulfilment of the requirements for the degree of Bachelor of Arts

April 2015

POMONA COLLEGE

Abstract

Dwight Whitaker
Physics and Astronomy

Bachelor of Arts

Ultracold Atoms in Line-World: Bose-Einstein Condensates in a Quasi-One Dimensional Gravito-Optical Surface Trap

by Benjamin Girodias

In recent experiments with lower dimensional Bose-Einstein condensates, ultracold atomic clouds are repelled upwards against the pull of gravity by the dipole force from an exponentially decaying evanescence wave in a confinement known as a gravito-optical surface trap. In the limit that the axial frequency is much less than the radial frequency, the condensate wavefunction is described by the quasi-one-dimensional form of the nonlinear Schrödinger equation called the Gross-Pitaevskii equation. Approximate Thomas-Fermi wavefunction solutions of this potential matched the numerical solutions found through propagation of a trial wavefunction in imaginary time using the split-step operator method. Strong agreement between the presented results and experimental vertical time of flight expansions validate these techniques.

Acknowledgments

I would like to recognize my collaboration with Javed Akram and Dr. Axel Pelster at the Freie Universität in Berlin. Here, I was introduced to my topic and received helpful insights that spurred the development of this work, especially with regards to the matlab code. I would also like to thank the DAAD RISE program for the financial support that allowed me to spend the summer in Berlin.

In addition, I would like to thank my professors at Pomona College whose support over the years has fostered my interest in physics. Beginning my research career with Dr. Richard Mawhorter, I learned the importance of focusing on detail as well as how to effectively collaborate with other scientists. I am also in debt to Dr. Dwight Whitaker who introduced me to the topic of quantum mechanics and Bose-Einstein Condensates. He is both an inspiring teacher as well as a wonderful mentor. Further, I would like to recognize Dr. David Tannenbaum for serving as my academic advisor over my four years at Pomona, guiding me toward academic success.

Lastly, I would like to thank my parents, Kathy and Ken Girodias, for instilling and supporting my interest in math and science from such an early age. Who knew that one preschooler summer camp about bats would take me this far?

Contents

List of Figures

Chapter 1

Introduction

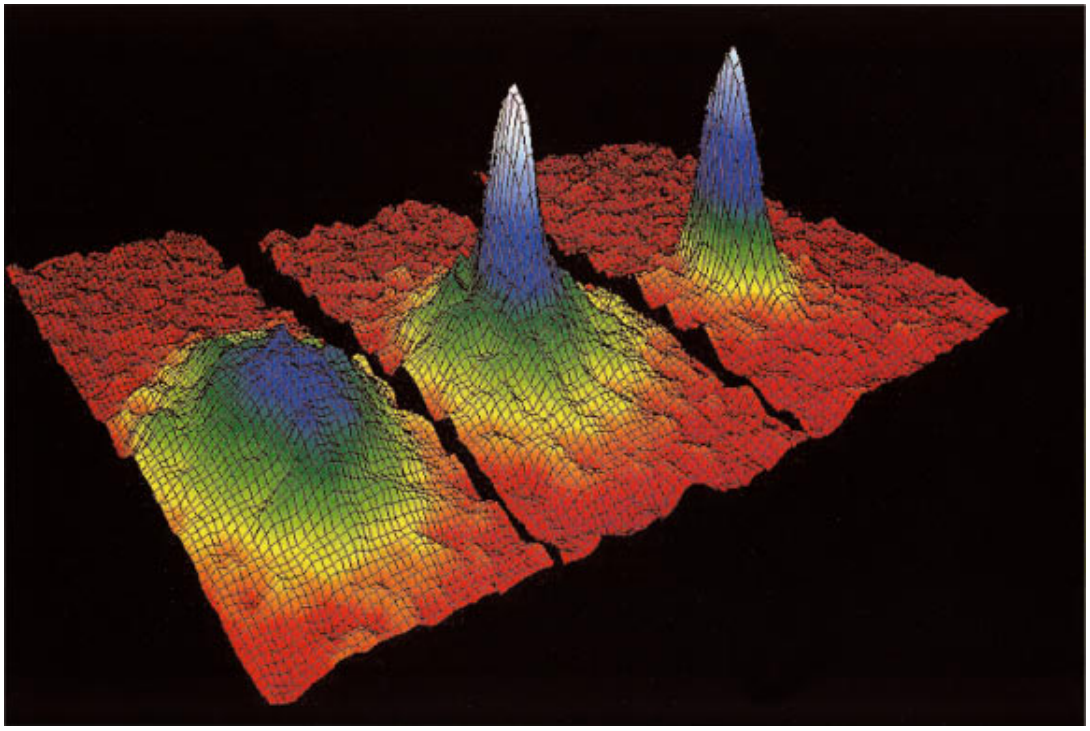

FIGURE 1.1: Velocity distribution of the atoms in the Anderson et. al. experiment [1]. The field of view is 200 μm $\times$270μm, see description of the image in Dafolvo et. al. [2].

1.1 Basics of Bose-Einstein Condensates

Image taking a bunch of atoms and slowly pressing them together while extracting heat from the system. At extremely low temperatures, the particles' wave nature becomes more pronounce and their de Broglie wavelength will begin to overlap at sufficiently high densities. Once this occurs, integer spin particles, called bosons, collapse to the same ground state, resulting in a Bose-Einstein condensate.

While BECs were first produced in 1995 [1, 3, 4], the theoretical predictions of this state of matter predated those experiments by some 70 years [5]. From first principle, Bose derived the statistical behavior of photons. Upon receiving his draft, Einstein personally translated it into German to be published in the *Zeitschrift für Physik* [6], and then he extended the idea to matter [7].

Although physicists realized that phenomenon such as superfluidity and superconductivity (where pairs of electrons form bosons) could be explained by partial condensation, these systems involved strong interactions, making theoretical calculations difficult [5]. The only clear path to make further progress in the experimental verification of Boson statistics was through the cooling of diffuse gases using lasers and magnetic fields.

Pioneered by 2001 Nobel Prize recipients, Cornell, Ketterle, and Wieman, the first successful BECs relied on lasers and magnetic fields to cool gases of alkali metals, such as Rb, Na, and even Li, down to hundreds of nanokelvin [5]. Because temperature is related to the velocity of the atoms; electromagnetic traps that slow down atoms also cool them. The experimental procedure is as follows: the atoms are initially placed in a more basic trap known as a Magneto-Optical Trap (MOT). A MOT is composed of six polarized axial beams and a quadrapole magnetic field. Together the lasers and magnetic field reduce the velocity of the atoms and confine them spatially. From the MOT, the atoms can be transfered into a more shallow optical dipole trap. The advantage of such a transfer is that the walls of the potential barrier can be lowered allowing only the most energetic particles to escape. Just like how steam removes thermal energy from a cup of coffee, the escaping energetic particles leave the remaining atoms at a lower temperature. Historically, this has also been accomplished by using radio frequency pulses to lower the potential barriers on a pure magnetic trap.

In addition to this conventional method, more recent experiments have trapped quasi-2D BECs in a gravito-optical surface trap (GOST) after first evaporative cooling with a dipole trap [8]. Based on the theoretical work of Cook [9], an upward evanescent wave (EW), produced by the total internal reflection on the underside of a prism, can be used to repel atoms vertically against the downward force of gravity. With a hollow laser beam confining the atoms in the radial direction, the gas is cooled in a process where gravitational potential energy is eventually radiated away in closed loop named Sisyphus cooling after the mythical king who was doomed to repeatedly push a rock up a hill [10]. By tightening the radial laser beam, the typical 2D cloud approaches the 1D limit and becomes cigar-shaped. This reduction in dimension has both interesting statistical and quantum properties.

Specifically, these tunable systems could be used as a model of liquid helium surfaces [8]. From a statistical mechanics point of view, the density of states is dependent on the

dimensionality of the system. Hence, the distribution function should be altered for lower dimensions. In either case, the development of a theoretical model for comparison will undoubtedly prove useful. Thus, to develop an expectation for realistic experimental results, the contents of this thesis theoretically investigates the spatial distribution of a BEC cloud confined in a quasi-1D GOST.

1.1.1 Outline of Thesis

This thesis will explore the wavefunction of a BEC in a quasi-1D GOST. Foremost, the theory necessary to model this system will be developed in Chapter 2. This will consist of first defining what a BEC is from a statistical mechanics point of view, then describing the experimental techniques necessary to produce them, and finally use mean field theory and basic quantum field theory to derive the Gross-Pitaevskii equation. Next in Chapter 3, the methods of finding the wavefunction of the BEC will be flushed out, beginning with the standard practice of nondimensionalizing the equation and then finding the form of the BEC wavefunction through analytic approximations and numerical methods. In Chapter 4, the results of the investigation will be presented, with a particular focus on relating these results back to on going experiments. Lastly, the results and methods will be summarized in Chapter 5.

Chapter 2

Theory

2.1 Statistical Mechanics of a BEC

We begin the derivation of the behavior of ultra-cold bosons by first reviewing the statistics of ordinary gases. Then I will highlighting the difference between them and their quantum counterparts.

For an ideal gas at room temperature, the Boltzmann distribution provides an accurate description of the macroscopic properties. In this scheme, the likelihood of a certain state with energy E_s at a temperature of T is given by

$$P(s) = \frac{1}{Z} e^{-E_s/k_B T}, \tag{2.1}$$

where $e^{-E_s/k_B T}$ is the Boltzmann factor, k_B is the boltzmann constant and Z is the partition function, which is the sum of all the Boltzmann factors for each state. For ordinary gases, the number of available states is much greater than the number of particles. Thus, we can assume that the probability of any two particles being in the same state is negligible, and so we can approximate the partition function for the entire system of N indistinguishable particles as

$$Z_{\text{Total}} = \frac{Z^N}{N!}, \tag{2.2}$$

where Z is the partition function for a single particle [11]. However at lower temperatures and higher densities, this assumption fails. In these regimes, the quantum mechanical behavior dictates how the particles interact. Half-interger spin particles called fermions cannot occupy the same state, whereas interger spin particles called bosons can have

any number in given state. The average number of atoms in a state of energy ϵ is called the distribution function. The graph for each of these three statistics can be seen in Fig 2.1. At ultra-low temperatures, the probabilistic clumping of bosons to the ground energy state leads to an interesting phase known as a Bose-Einstein condensate.

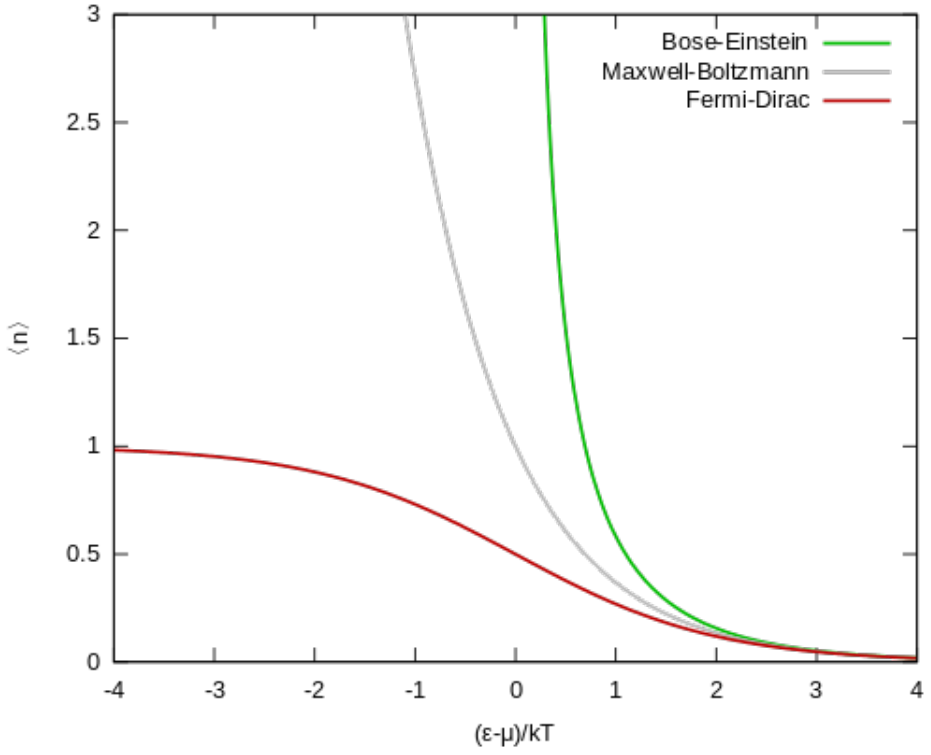

FIGURE 2.1: The distribution functions for Bose-Einstein, Fermi-Dirac, and Boltzmann statistics. Note how for higher temperatures, the three distributions converge. ϵ is the energy of a given state and μ is the chemical potential as described in Eq. 2.3

2.1.1 Bose-Einstein Statistics

In order to derive the Bose-Einstein distribution functions, the classical description must be extended to include the possibility of exchanging particles with a reservior. This modification results in a transformation from the Boltzmann factor to the Gibbs factor, which can be written as $E_s \rightarrow E_s - \mu N_s$ where μ is the chemical potential and N_s is the number of particles in state s. Formally, the chemical potential relates the change in Gibbs free energy G to the change in N at constant temperature and pressure as

$$\mu = \left(\frac{\partial G}{\partial N}\right)_{T,P}. \tag{2.3}$$

This leads to the grand partition function $\mathcal{Z}$ given by

$$\mathcal{Z} = \sum_s e^{-(E_s - \mu N_s)/k_B T} \tag{2.4}$$

For bosons in contact with a reservior of a constant temperature and chemical potential (the grand canonical ensemble), the energy of a state with N particles is $N\epsilon$, where ϵ is the energy of the excited state. For realistic physical systems, the Gibbs factors must be finite, meaning $\epsilon > \mu$. Thus, the grand partition function for this system where any number of particles can be in each state is given by

$$\mathcal{Z} = \sum_{n=0}^{\infty} e^{-n(\epsilon-\mu)/k_B T} = \frac{1}{1 - e^{-(\epsilon-\mu)/k_B T}} \tag{2.5}$$

because the the sum of any infinite geometric series with $r < 1$ is $\sum_{i=0}^{\infty} r^i = 1/(1-r)$.

The expected number of atoms in each state is $\bar{n} = \sum_{n=0}^{\infty} nP(n)$, where $P(n)$ is the probability of a state with n particles. Note that $P(n) = (1/\mathcal{Z})e^{-n(\epsilon-\mu)/k_B T}$. Also, for $|r| < 1$, the exists the formula $\sum_{i=0}^{\infty} ir^i = r/(1-r)^2$. Thus,

$$\begin{aligned} \bar{n} &= \sum_{n=0}^{\infty} n \frac{1}{\mathcal{Z}} e^{-n(\epsilon-\mu)/k_B T} \\ &= -\left(e^{-(\epsilon-\mu)/k_B T} - 1\right) \sum_{n=0}^{\infty} n e^{-n(\epsilon-\mu)/k_B T} \\ &= \frac{e^{-(\epsilon-\mu)/k_B T}}{1 - e^{-(\epsilon-\mu)/k_B T}} = \frac{1}{e^{(\epsilon-\mu)/k_B T} - 1} \end{aligned} \tag{2.6}$$

This indicates that as $\epsilon \to \mu$, $\bar{n} \to \infty$, suggesting that at extremely low temperatures, large number of atoms collapse to the ground state.

2.1.2 Critical Temperature

To find the number of atoms in a BEC, we first derive the density of states for a system at a given energy. With this information, the number of atoms in a given energy state can be found by summing the product of the distribution function ($\bar{n}$) and the density of state $g(E)$ for each energy. Assuming a continuous distribution of the energy states will simplify the calculation.

Based on Einstein's original paper [7], the density of states will be found by quantizing the phase volume Φ, which is given by

$$\Phi = \int \mathrm{d}x\ \mathrm{d}y\ \mathrm{d}z\ \mathrm{d}p_x\ \mathrm{d}p_y\ \mathrm{d}p_z = V\frac{4}{3}\pi(2mE)^{3/2} \tag{2.7}$$

for a volume V and an energy $E = p^2/2m$ in the absence of an external potential. The density of states is simply the number of energy states in the phase volume between E and $E + \mathrm{d}E$. Because the density of states is quantized in units of h^3 and must have units of $1/[\text{Length}]^3$, we see that

$$g(E) = \frac{1}{h^3}\ \mathrm{d}\Phi = \frac{2}{\sqrt{\pi}}\left(\frac{2\pi m}{h^2}\right)^{3/2} V\sqrt{E}\ \mathrm{d}E. \tag{2.8}$$

With a small step size ($k_B T \gg E_0$), the number of atoms N in our collection is given by

$$N = \int g(E)\bar{n}(E)\ \mathrm{d}E, \tag{2.9}$$

as this is the sum of the number of atoms per state times the number of states per energy over each energy state. We can complete this calculation once we know the chemical potential. In particular consider what occurs when a cloud of bosons begin to condensate. Once this occurs, adding another boson will not add any energy because it joins the ground state. Hence $\mu = 0$ at the critical temperature T_c when the condensate begins to form.

With the substitution $x = E/k_B T$ the integral becomes

$$N = \int_0^\infty \frac{2}{\sqrt{\pi}}\left(\frac{2\pi m k_B T}{h^2}\right)^{3/2} V\sqrt{x}\frac{1}{e^x - 1}\ \mathrm{d}x \text{ at } T = T_c\ . \tag{2.10}$$

Preforming this integral with the aid of computational tools, the above simplifies to

$$\frac{N}{V} = 2.612\left(\frac{2\pi m k_B T}{h^2}\right)^{3/2} \text{ at } T = T_c\ , \tag{2.11}$$

but strangely $\mu = 0$ for $T < T_c$ as well. This seems to imply that the number of atoms is a function of the temperature. However, note how the approximate density of state (see Eq. 2.8) has zero states when $E = 0$. Hence, the derivation shows that the atoms in our condensate will be in the excited state until this critical temperature. Below this point, the integral approximation only accounts for the atoms in the excited states N_{exc}.

So, the number of atoms in the ground state N_0 shown in Fig 2.2 is given by

$$\frac{N_0}{N} = 1 - \frac{N_{exc}}{N} = 1 - \left(\frac{T}{T_c}\right)^{3/2} \text{ for } T < T_c\ . \tag{2.12}$$

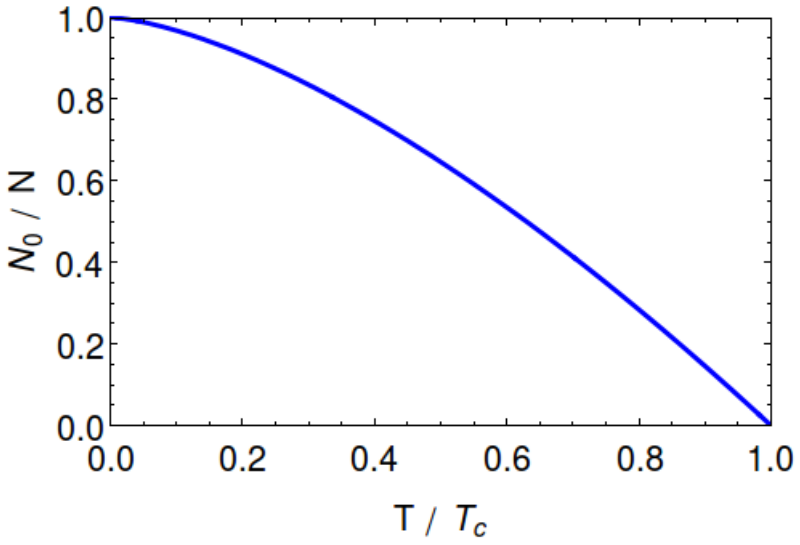

FIGURE 2.2: This diagram shows how the number of atoms in the ground state increase as the temperature decreases.

For a more intuitive understanding, this critical temperature occurs when atoms begin to overlap. Defining the de Broglie wavelength as $\lambda_{dB} = h/\sqrt{2\pi m k_B T}$, Eq. 2.12 can be expressed in terms of the phase space density $\rho = (N/V)\lambda_{dB}^3$ as

$$\frac{N_0}{N} = 1 - \frac{2.612}{\rho} \text{ for } T < T_c \tag{2.13}$$

In this way, condensation begins when $N_0 = 0$ or $\rho \geq 2.612$. This corresponds to the intersection of the atom spheres of radius λ_{dB}. Note how this overlap only occurs at ultra-low temperatures because the $\lambda_{dB} \propto 1/\sqrt{T}$. For comparison, regular air at standard temperature ($T = 273K$) and pressure (1 atm), the phase space density is on the order of 10^{-7}, which is over a million times too diffuse.

2.2 Experimental Construction

Experiments in 1930s and 1940s with liquid helium displayed some odd properties that could not be explained classically, such as superfluidity. Under H. London's suggestion, these novel properties might be explained by partial condensation in liquid helium [2]. However, the strong interactions between helium atoms made theoretical analysis near impossible. Thus, the motivation to confirm the quantum statistics drove experimentalists to try to find a ultra-cold system of weakly interacting particles where BECs could be produced and manipulated. This led to the development of atom trapping techniques described below.

2.2.1 Magneto-Optical Trap

In order to trap something, the object must be stopped and held at a certain position. For example, when a outfielder makes a catch, his or her glove dampens the kinetic energy of the ball while the player's grip retains the ball in the middle of the glove. Unlike the ball's motion, atoms in a gas move randomly, so a successful trap confines the atoms in both velocity and position space from all directions. The initial confinement is almost always done with a MOT because they are low cost and relatively simple to set up. In fact, Wieman et al. showed that this atom trapping can be accomplished for as little as $3000 [12].

There are three main components to a MOT: the vacuum system, six orthogonal polarized laser beams, and a quadrapole magnetic field, see Fig 2.3. The vacuum system is needed to stop collisions of the trapped atoms with room temperature atoms. Such collisions thermalize the atoms, meaning that the transfer of momentum from these hotter atoms would allow the cold atoms to escape the trap.

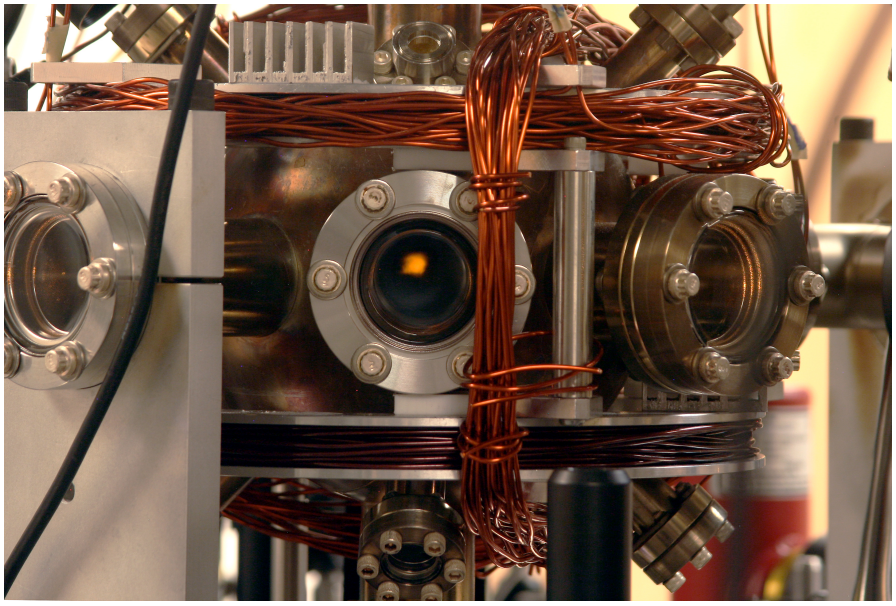

FIGURE 2.3: A long exposure picture of a MOT produced in Dr. Dwight Whitaker's lab [13]. The orange glowing spec inside the chamber is an ultra-cold cloud of atoms.

The atoms are slowed down through a process suggestively called optical molasses. For simplicity in this description, imagine the atoms are idealized with only two energy levels. In reality, one must include another repump laser to reduces the losses of atoms that transition to a third dark state, but this complication can be ignored for now. Each of the six laser beams are slightly red detuned from resonant frequency. In this way, as atoms travel in the opposite direction of a laser beam, the relative velocity doppler shifts the frequency of the laser to resonance. As a result, the atom absorbs the photon's

momentum, thereby reducing its speed. At this point, the atom spontaneously emits a photon in a random direction. Because no direction of emission is prefered, the average kick from this emission is zero. Hence, the atoms will get slowed only when they travel against a laser beam's propagation direction. As this cooling relies heavily on the doppler effect, it is also known as Doppler cooling. Note that the atoms moving with the beam will see the frequency even further red shifted, so they are not likely to absorb those photons.

The position confinement could be called Zeeman trapping. The quadrapole magnetic field produced by two anti-Hemholz coils provides a field that is about linear with displacement from the origin along each axis, see Fig 2.4. Due to the Zeeman effect, the magnetic field splits the the energy level of the atoms. In Fig 2.4, we see that if the atom moves along the positive z-axis, then the state M_- has less energy. So, the atom will be more likely to absorb the photon in the σ_- state, which is coming from $+\infty$. Thus, if the atom is displaced from the center of the trap, it will be likely to be kicked back toward the center even if its velocity is zero. Further, note how if the atom is at the origin, then atom experiences no magnetic field shift, so there is no prefered absorbtion of any of the laser beams. This means when it has a low velocity, it will remain at the that position.

Though impressive for the cost, the trapped atoms inside a MOT cannot reach the conditions necessary for a BEC. The atomic density n is limited to around $10^{11}/\text{cm}^3$ because of the pressure of the emitted photons [10]. The spontaneously emitted photons from an inner atom always push outwards on the other atoms so that they can never get denser. At this maximum density, the atoms would need to have a temperature on the order of a few nK to form a BEC, which is far beyond the μK temeperatures achievable by the these MOTs.

2.2.2 Sub-doppler Cooling

From this point, the atoms are transfered to an alternate trap, whose potential barriers can be slowly lowered. In doing so, the more energetic particles are allowed to escape, thereby cooling off the remaining atoms. This process has been named evaporative cooling for its similarity to how a cup of coffee cools down. The two most common traps are a time orbiting potential (TOP) magnetic trap [1] and an optical dipole trap [14].

The magnetic traps take advantage of the natural magnetic dipole of neutral atoms. The force on a magnetic dipole is given by

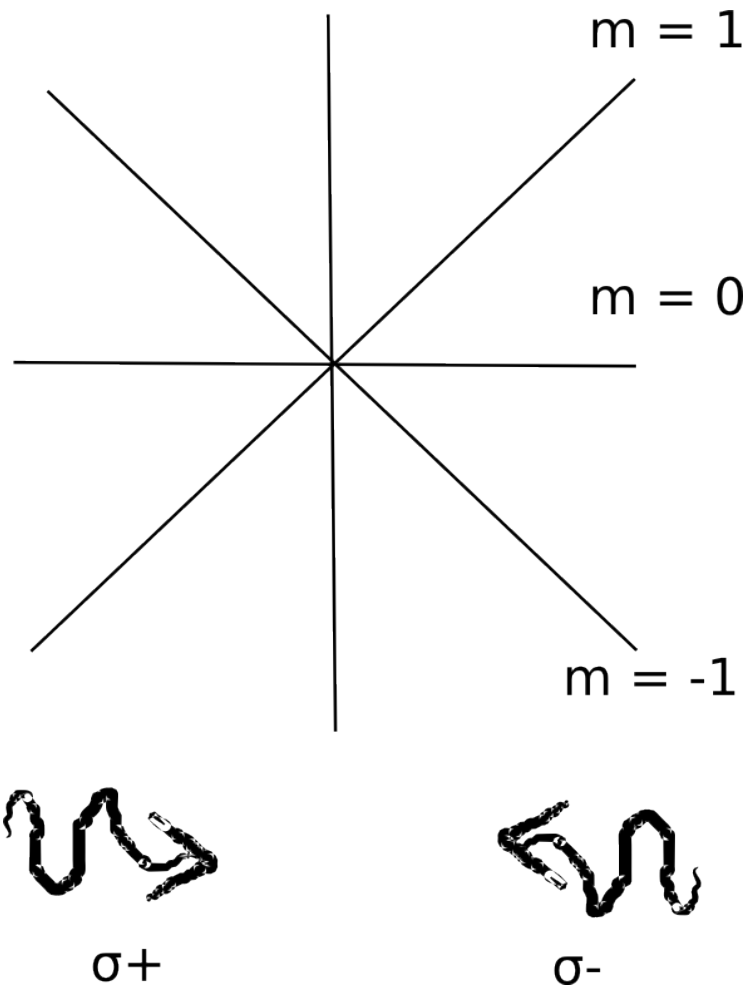

FIGURE 2.4: The magnetic field as a linear function of position. As the atom moves away from the origin its energy level is shifted by the Zeeman effect. Thus, it is more likely to absorb the photon that will push it back toward the origin.

$$\vec{F} = \vec{\nabla}(\vec{\mu} \cdot \vec{B}) \tag{2.14}$$

where $\vec{F}$ is the force, $\vec{\mu}$ is the magnetic moment, and $\vec{B}$ is the magnetic field. For a constant $\vec{\mu}$, the trap requires a magnetic field with a nonzero derivative. Initially, the quadrapole trap of the MOT might seem like a feasible candidate, but this is inadequate because $\vec{B} = 0$ at the origin. Here, the atom's spin orientation may flip. With the opposite magnetic moment these flipped atoms will actually be repelled rather than trapped. By rotating the zero field location around the cloud of atoms in a uniform manner see Fig. 2.5, the time average bias field is nonzero and such nonadiabatic spin-flips do not occur [15].

Already, the TOP provides a mechanism for evaporative cooling on its own, as the faster moving particles can reach the zero potential point and flip their spins. To continue the

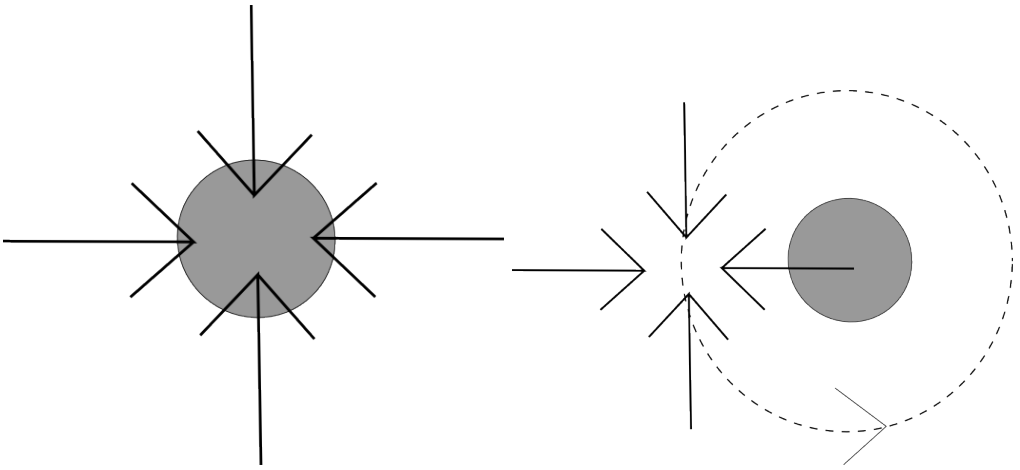

(A) Quadrapole trap (B) TOP trap

FIGURE 2.5: Adapted from Ref [15]. Here the difference between the ordinary quadrapole trap and the TOP trap that has the cyclically changing bias field.

process, applied RF pulses alter the spins of particles with a high Zeeman shift, which corresponds to those with more energy and are farther from the center of the trap. In this manner, the detuning of the RF can slowly be decreased toward resonance, releasing only the most energetic atoms. Eventually, this interative process of rethermalization and then RF pulsing will lead to the critical density necessary to form a BEC.

Alternatively, a pure optical dipole trap can be achieved using a single highly focused Gaussian beam. The radial intensity $I(r)$ varies as

$$I(r) = I_0 e^{-r^2/\omega_0^2} \tag{2.15}$$

with ω_0 is the beam waist size (at the focus, the beam is about $2\omega_0$ in width). The basis of this dipole force can be imagined as a two part process in a standing wave, see Fig. 2.6: the atom absorbs the momentum of one of the components and then relases a stimulated emission photon from the other component of the standing wave [10].

This relies heavily on the the gradient of the beam's intensity; hence, the necessity of a high power lens to focus the beam. Spcifically when the detuning is much greater than the Rabi frequency Ω and spontaneous decay rate γ, the force F is approximated as

$$F(r) \approx -\frac{\hbar\gamma^2}{8\delta I_s}\nabla I(r) \tag{2.16}$$

where $\delta = \omega_{\text{laser}} - \omega_{\text{res}}$ is the detuning and I_s is the saturation intensity. To overcome the radiation pressure along the axis, a large detuning δ is required, noting that the dipole

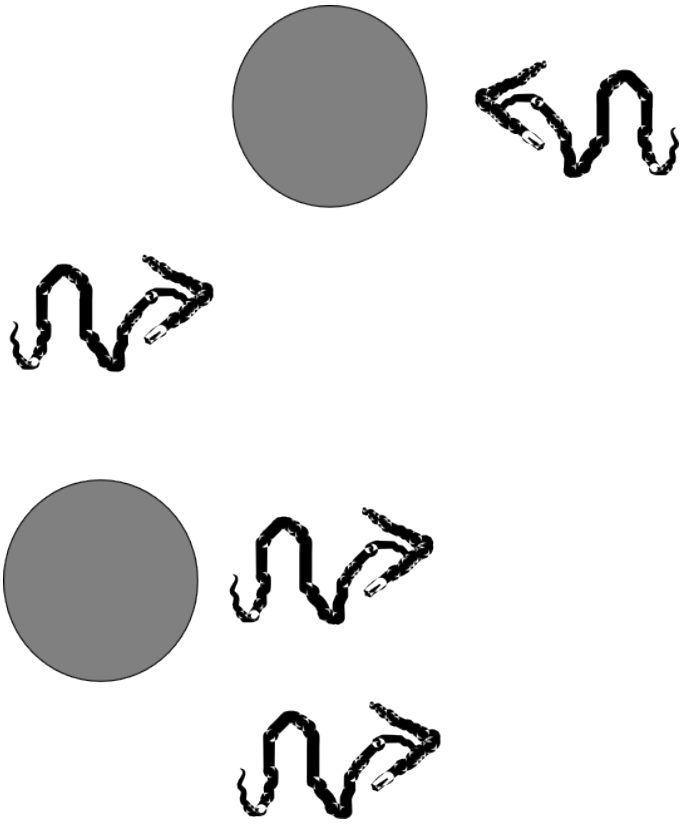

FIGURE 2.6: The two part process of the dipole force where the atom absorbs one photon and then emits another through stimulated emission in the opposite direction to that of the absorbed photon. This process depends on the gradient of the potential as noted in Eq. 2.16

force falls as $1/\delta$, while the radiative force falls as $1/\delta^2$ [10]. Typically a CO_2 laser with a wavelength of 10.6 μm is used to confine ^{87}Rb atoms with a resonance wavelength of 780 nm.

The intensity of the trapping beam is reduced to evaporatively cool the atoms. Because the force is proportional to the laser intensity, see Eq. 2.16, the simplest way of reducing the force is to reduce the power output of the laser. Unfortunately, this will also lower the trap frequency and, as a result, the rate of thermalization [14]. Often though, the trap can be designed so that the evaporated particles take away enough energy so that the critical densities can still be obtained.

2.2.3 Gravito-Optical Surface Traps

Recent experiments have used a GOST to confine quasi 2D clouds of atoms [8]. In this experiment, the atoms are confined initially with a MOT and then dropped into the

GOST. The GOST consists of a hollow radially confining beam and an EW along the vertical axis, see Fig. 2.7

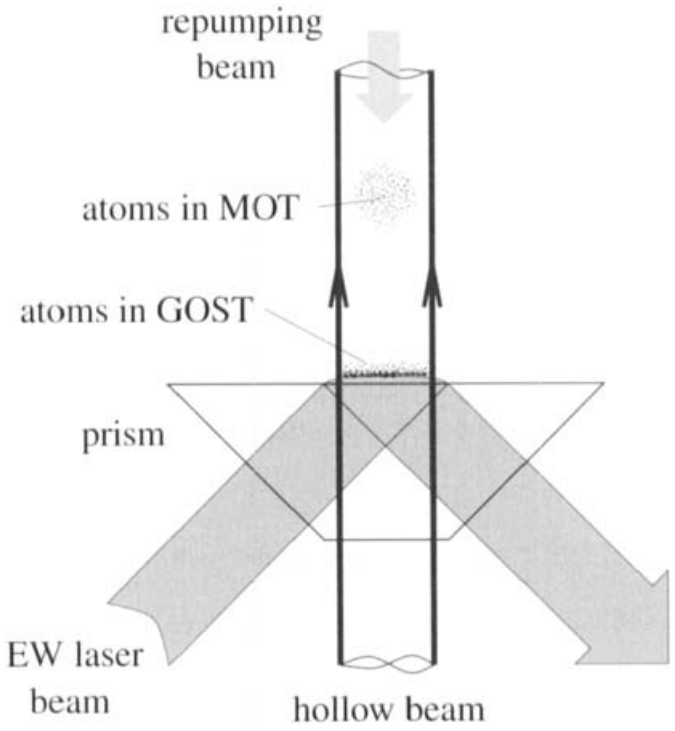

FIGURE 2.7: Experimental set-up of a GOST from Ref. [16]. The downward pull of gravity is compensated by the repulsive dipole force of the EW.

The strong gradient of the hollow beam provides the mechanism for the dipole force to push atoms back toward the axis. Along the vertical z-axis, the laser beam bouncing off the underside of the prism produces an EW from the total internal reflection [9]. Essentially, the boundary conditions of the electric field demands the existance of the EW for a continuous solution to Maxwell's equations. The atoms are cooled through a Sisyphus mechanism that relies on three energy levels of the atoms, the blue-shifted EW wave and the repumping beam, see Fig. 2.8 [10]. For Cs atoms, the lower hyper-fine levels are $F = 3$ and $F = 4$, which are separated by $\delta/2\pi = 9.2$GHz.

This cyclic process of kinetic energy to potential energy and then radiating away that gained potential energy is called Sisyphus cooling after the mythical figure, who was doomed to continue to push a rock up a hill only to watch it roll back down. Like Sisyphus, the atoms gain potential energy, but they do so by making a transition in the EW field. They are optically pumped from $F = 3$ to the excited state and then back to $F = 4$. Like a ball that loses some of its kinetic energy while bouncing on a surface, the atoms are projected upward, but do not rise to their original height. Further, a downward directed repump beam further their kinetic energy through radiation pressure

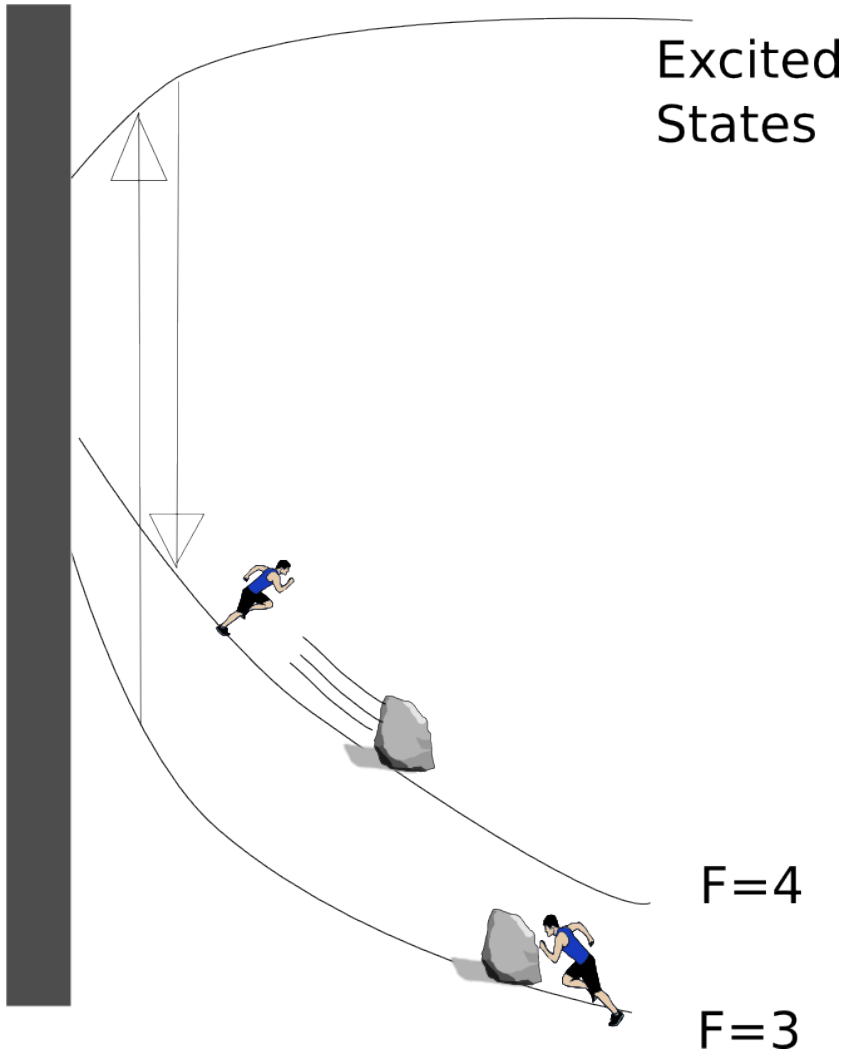

FIGURE 2.8: Adopted from [10]. This shows the transition the atoms make from kinetic to potential, which is eventually radiated away. Near $z = 0$, the dark bar, the atoms' energy levels are shifted making the transition from $F = 3$ to the excited state back down to $F = 4$ possible. This results in a transfer of kinetic energy to internal energy. The repump beam (not shown) makes the transistion back to the lower ground state ($F = 3$), thereby radiating away the gained potential energy. Superimposed upon the image is a depiction of the mythological analogy.

and optically transitions the atoms back down to the $F = 3$. So, the atoms have made a complete refrigeration loop and continue to do so until they reach an equilibrium.

Although this process does cool the atoms, Grimm's group ultimately confined the atoms in their GOST and employed a dipole trap to reach the necessary critical density [8].

2.3 Theoretical Description of a Quasi-1D GOST

In the experimental lab, the atoms are not the idealized noninteracting particles described in section 2.1. While the atomic forces upon one another can be quite complicated, in certain regimes of densities, the mean field approximation can be used, yielding the Gross-Pitaevskii (GP) equation.

This section will first introduce the ideas of quantum field theory as they apply directly to the derivation of the GP equation. Next, the GP equation will be applied the lower dimensional collections of atoms.

2.3.1 Basics of Quantum Field Theory

In the late 1800's black body radiation from harmonic oscillators seemed to match the Jeans-Rayleigh empirical relation quite well at lower frequencies. However, this empirical law led to the ultraviolet catastrophe where the emitted radiation was to approach infinity as the wavelength decreased. Certainly, this is not physically realistic. In 1901, Max Plank proposed that the energy of the oscillator was quantized, and with this prediction he showed that this catastrophe could be adverted. Later, P. A. M. Dirac showed the electromagnetic (EM) field has the same form as a collection of oscillators, explicitly seen with a clever change in variables [17]. Insightfully, he suggested that these variables were actually noncommunicative operators, thereby quantizing the EM field.

As explained in [18] and [17], the quantization of the EM field leads to the prediction of a discrete number of photons. Foremost, the following description uses the vector potential $\vec{A}$ rather than the electric $\vec{E}$ or the magnetic $\vec{B}$ fields as the more fundamental quantity. In essence, this stems from the interesting results of the Aharonov-Bohm effect where the interference pattern of a double slit experiment is altered by the magnetic field of a solenoid, see Fig. 2.9.

Although, the most probable particle paths do not cross the magnetic field ($\vec{B}$ is contained within the infinite solenoid) the relative phase of the particles is still affected [17]. Succinctly, this strange result can be understood through Feynmann's path integral technique where the amplitude of a particle being at a position x_f at time t_f from the position x_0 at the initial time t_0 can be determined by taking the integral of $e^{iS[x(t)]/\hbar}$ along each possible path where S is the action defined as

$$S[x(t)] = \int_{t_0}^{t_f} dt\ L(x, \dot{x}) \tag{2.17}$$

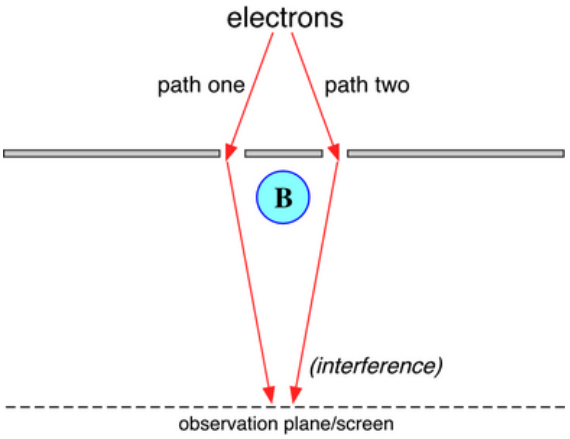

FIGURE 2.9: Diagram of the Aharonov-Bohm thought experiment. Notice how the dominate particle paths do not cross through the magnetic field contained within the solenoid. However, they particle's phase is affected by the vector potential, which is outside the solenoid.

Note that L is the Lagrangian. In the case of this experiment, the Lagrangian is $L = 1/2m(\dot{\vec{x}})^2 - q\varphi + (q/c)\vec{A}\cdot\dot{\vec{x}}$ [17], where φ is the scalar potential and $\vec{A}$ is the vector potential with $\vec{B} = \nabla \times \vec{A}$. Along the different paths, the introduction of the magnetic field introduces a phase of

$$\text{phase} = \exp\left(i\frac{q}{\hbar c}\int_{t_0}^{t_f} \vec{A}\cdot d\vec{x}\right), \tag{2.18}$$

as $\dot{\vec{x}}\, dt = d\vec{x}$. So along the two dominate paths, the relative phase difference is given by

$$\begin{aligned}\text{relative phase} &= \exp\left(i\frac{q}{\hbar c}\int_{\text{path 1}} \vec{A}\cdot d\vec{x}\right) - \exp\left(i\frac{q}{\hbar c}\int_{\text{path 2}} \vec{A}\cdot d\vec{x}\right) \\ &= \exp\left(i\frac{q}{\hbar c}\oint \vec{A}\cdot d\vec{x}\right) \\ &= \exp\left(i\frac{q}{\hbar c}\int \vec{B}\cdot d\vec{S}\right)\end{aligned} \tag{2.19}$$

by Green's theorem. So, the interference pattern of the experiment is indeed dependent on the magnetic flux. Although the treatment of the EM field has been classical so far, the above derivation does illustrate the importance of the vector potential for quantum phenomenon.

Now, consider a region in which there is no charge or current. Writing Faraday's law in gaussian units in the form $\nabla \times \left(\vec{E} + (1/c)(\partial\vec{A}/\partial t)\right) = 0$, then the classical Hamiltonian H for such a region is defined as

$$H = \frac{1}{8\pi}\int dV(\vec{E}^2 + \vec{B}^2) = \frac{1}{8\pi}\int dV\left[\left(-\frac{1}{c}\frac{\partial\vec{A}}{\partial t}\right)^2 + \left(\nabla\times\vec{A}\right)^2\right] \tag{2.20}$$

Because the physical field $\vec{B} = \nabla \times \vec{A}$, then adding the gradient of a scalar $\nabla\alpha$ doesn't affect the value of $\vec{B}$ since $\nabla \times \nabla\alpha = 0$ for any scalar function α. This is known as guage freedom. In the Coulumb gauge where $\nabla \cdot \vec{A} = 0$, ie setting $\nabla^2\alpha = -\nabla \cdot \vec{A}$, Ampére's law becomes in the absence of charge [17],

$$\frac{1}{c^2}\frac{\partial^2 \vec{A}}{\partial t^2} - \nabla^2 \vec{A} = 0. \tag{2.21}$$

Based on the approach of Sakurai, the solution to this wave equation at the initial time will be expanded as a Fourier series of plane waves, assuming periodic boundary conditions of a cube with length $L = (V)^{1/3}$ [18]. This yields

$$\vec{A}(x,t) = \frac{1}{\sqrt{V}} \sum_{\vec{k},s} \left[c_{\vec{k},s}\vec{\epsilon}(\vec{k},s)e^{i(\vec{k}\cdot\vec{r}-\omega t)} + c^*_{\vec{k},s}\vec{\epsilon}(\vec{k},s)e^{-i(\vec{k}\cdot\vec{r}-\omega t)} \right], \tag{2.22}$$

where $\vec{k}$ is the wave vector, $\omega = |\vec{k}|c$ is the frequency, $\vec{\epsilon}$ is the polarization vector of two possible directions $s = 1$ and $s = 2$, and $c_{\vec{k},s}$'s are the coefficients of the expansion. Due to the fact $\nabla \cdot \vec{A}$, the Coulumb guage implies $\vec{\epsilon} \perp \vec{k}$, so it is often called the transverse guage, as $\vec{A}$ is perpendicular to the propagation direction of the wave.

This boundary condition means that for each dimension, j, $e^{ik_j x_j} = e^{ik_j(x_j+L)}$. Hence, there exists the orthonormality relation of the form

$$\int d^3r \; \frac{e^{-i\vec{k}\cdot\vec{r}}}{\sqrt{V}} \frac{e^{i\vec{k}'\cdot\vec{r}}}{\sqrt{V}} = \delta_{\vec{k},\vec{k}'} \tag{2.23}$$

where the kronecker delta $\delta_{\vec{k},\vec{k}'} = 1$ if $\vec{k} = \vec{k}'$ and is otherwise zero.

Still, the derivation has been treating the electromagnetic field classically. In the quantum mechanical world, the Hamiltonian must be an operator, ie $H \to \hat{H}$, on a wavefunction. It is clear that if the left side of Eq. 2.20 is now an operator, then we must write the vector potential as an operator as well. Thus, with insight the substitutions

$$c_{\vec{k},s} \to c\sqrt{\frac{2\pi\hbar}{\omega}}\hat{a}_{\vec{k},s} \qquad\qquad c^*_{\vec{k},s} \to c\sqrt{\frac{2\pi\hbar}{\omega}}\hat{a}^\dagger_{\vec{k},s} \tag{2.24}$$

are applied to Eq. 2.22 leading to a quantized field $\hat{\mathbf{A}}$. Carrying out this substitution into Eq. 2.20 and using the orthonormality relations, the quantized Hamiltonian reduces to

$$\hat{H} = \frac{1}{2}\sum_{\vec{k},s} \hbar\omega \left(\hat{a}^\dagger_{\vec{k},s}\hat{a}_{\vec{k},s} + \hat{a}_{\vec{k},s}\hat{a}^\dagger_{\vec{k},s} \right), \tag{2.25}$$

which takes the exact same form as the quantum harmonic oscillator [17]! With this analogy in mind, the operators are presumed to satisfy the commutator relations

$$\begin{aligned}[\hat{a}_{\vec{k},s}, \hat{a}^{\dagger}_{\vec{k}',s'}] &= \delta_{\vec{k},\vec{k}'}\delta_{s,s'} \\ [\hat{a}_{\vec{k},s}, \hat{a}_{\vec{k}',s'}] &= 0 \\ [\hat{a}^{\dagger}_{\vec{k},s}, \hat{a}^{\dagger}_{\vec{k}',s'}] &= 0\end{aligned} \tag{2.26}$$

where for operators $\hat{P}$ and $\hat{Q}$, $[\hat{P}, \hat{Q}] = \hat{P}\hat{Q} - \hat{Q}\hat{P}$.

With these relations, the Hamiltonian can be further simplified to

$$\hat{H} = \sum_{\vec{k},s} \hbar\omega \left(\hat{a}^{\dagger}_{\vec{k},s} \hat{a}_{\vec{k},s} + \frac{1}{2} \right). \tag{2.27}$$

The operators $\hat{a}_{\vec{k},s}$ and $\hat{a}^{\dagger}_{\vec{k},s}$ are the annihilation and creation operators respectively. As the name suggests, these operators are responsible for introducing a new quantized bit of the EM field in a state with a wave vector $\vec{k}$ and spin state s, i.e. a photon.

The annihlation operator destroys one photon, so that

$$\hat{a}_{\vec{k},s} \left| n_{\vec{k},s} \right\rangle = \sqrt{n_{\vec{k},s}} \left| (n-1)_{\vec{k},s} \right\rangle, \tag{2.28}$$

where $|n_{\vec{k},s}\rangle$ denotes the number of atoms in a certain state specified by s and $\vec{k}$. Naturally, if the annihilation operator acts on a state with no photons called the vacuum state $|0\rangle$, then $\hat{a}_{\vec{k},s} |0\rangle = 0$.

On the other hand, the creation operator introduces a new photon as

$$\hat{a}^{\dagger}_{\vec{k},s} \left| n_{\vec{k},s} \right\rangle = \sqrt{n_{\vec{k},s} + 1} \left| (n+1)_{\vec{k},s} \right\rangle \tag{2.29}$$

These are postulated in such a way that the number operator $\hat{N} = \hat{a}^{\dagger}_{\vec{k},s} \hat{a}_{\vec{k},s}$ gives the number of photons in a given state $\vec{k}, s$ because

$$\hat{N} \left| n_{\vec{k},s} \right\rangle = \hat{a}^{\dagger}_{\vec{k},s} \hat{a}_{\vec{k},s} \left| n_{\vec{k},s} \right\rangle = \hat{a}^{\dagger}_{\vec{k},s} \sqrt{n_{\vec{k},s}} \left| (n-1)_{\vec{k},s} \right\rangle = n_{\vec{k},s} \left| n_{\vec{k},s} \right\rangle \tag{2.30}$$

Operating the Hamiltonian on the vacuum state $|0\rangle$ highlights the strangeness of the quantum world. The energy of the system is the eigen value to the Hamiltonian operator. Note that $\hat{N} |0\rangle = 0$, so the energy of the vacuum is

$$E_0 = \frac{1}{2} \sum_{\vec{k},s} \hbar\omega. \tag{2.31}$$

Unfortunately, this value diverges, but since the physical applications depend only on the difference in energy, this value can be treated as if it were finite. The attraction of two neutral metal plates in a vacuum, called the Casimir effect, illustrates this odd result [17]. Because only certain wavelegnths can fit into a given cavity, the zero point energy inside is less than outside resulting in a non-constant potential energy, which produces a force inward (recall $F = -\nabla U$).

2.3.2 Many Atoms and Mean Field Theory

As photons are a type of boson, the past development of the creation and annihilation operators will be generalized for bosons in general.

Rather than using the wave vector and spin to specifiy the state of the general boson, the state of the boson is denoted simply with a subscript number. The collection of the spaces containing $0, 1, 2, ...$ particles is known as the Fock space [19]. This means that

$$|n_1, n_2, n_3, ...\rangle = |n_1\rangle\,|n_2\rangle\,|n_3\rangle\,... \tag{2.32}$$

with the vacuum space remaining $|0\rangle$.

To create a particle at a specific position, the eigenstate $|\vec{x}\rangle$, the creation and annihilation operators are introduced as respectively, adopting the notation $\vec{r} = \mathbf{r}$,

$$\begin{aligned} \hat{\Psi}^\dagger(\mathbf{r}) &= \sum_i \phi_i^*(\mathbf{r})\hat{a}_i^\dagger \\ \hat{\Psi}(\mathbf{r}) &= \sum_i \phi_i(\mathbf{r})\hat{a}_i, \end{aligned} \tag{2.33}$$

where $\phi_i(\mathbf{r})$ is the wavefunction for a single particle [19].

The Hamiltonian for a collection of boson consists of the kinetic term, potential term, and an interaction term between the bosons. From its similarity to the nonlinear-Schrödinger equation, the method used here is known as second quantization. Thus, in the most general form,

$$\begin{aligned} \hat{H} = \int d^3\mathbf{r}\ \hat{\Psi}^\dagger(\mathbf{r}) \left(-\frac{\hbar^2}{2m}\nabla^2\right) \hat{\Psi}(\mathbf{r}) + \int d^3\mathbf{r}\ \hat{\Psi}^\dagger(\mathbf{r}) U(\mathbf{r}) \hat{\Psi}(\mathbf{r}) + \\ \frac{1}{2}\int d^3\mathbf{r}\ d^3\mathbf{r}'\ \hat{\Psi}^\dagger(\mathbf{r})\hat{\Psi}^\dagger(\mathbf{r}')V(\mathbf{r}-\mathbf{r}')\hat{\Psi}(\mathbf{r}')\hat{\Psi}(\mathbf{r}). \end{aligned} \tag{2.34}$$

In this form, the terms in Eq. 2.34 represent the kinetic, potential, and interaction terms from left to right.

The kinetic term can be simplified by

$$\int d^3\mathbf{r}\ \hat{\Psi}^\dagger(\mathbf{r})\left(-\frac{\hbar^2}{2m}\nabla^2\right)\hat{\Psi}(\mathbf{r}) = \frac{\hbar^2}{2m}\int d^3\mathbf{r}\ \nabla\hat{\Psi}^\dagger(\mathbf{r})\cdot\nabla\hat{\Psi}(\mathbf{r}) \tag{2.35}$$

from the vector calculus identity $a\nabla^2 b = \nabla\cdot(a\nabla b) - \nabla a\cdot\nabla b$, and the fact that the other volume integral can be converted to surface integral whose argument namely $\hat{\Psi}^\dagger(\mathbf{r})\nabla\hat{\Psi}(\mathbf{r}) \to 0$ at infinity [19].

In the Heisenberg picture, the states are constant, so

$$\hat{\Psi} = e^{i\hat{H}t/\hbar}\hat{\Psi}(\mathbf{r},0)e^{-i\hat{H}t/\hbar}. \tag{2.36}$$

The time dependence of the operator satisfies the relation

$$i\hbar\frac{\partial\hat{\Psi}}{\partial t} = -[\hat{H},\hat{\Psi}] \tag{2.37}$$

It will be helpful to note the commutator relations for the field operators is as follows

$$\begin{aligned}[\hat{\Psi}(\mathbf{r}),\hat{\Psi}(\mathbf{r}')] &= [\hat{\Psi}^\dagger(\mathbf{r}),\hat{\Psi}^\dagger(\mathbf{r}')] = 0\\ [\hat{\Psi}(\mathbf{r}),\hat{\Psi}^\dagger(\mathbf{r}')] &= \sum_{i,j}\phi_i(\mathbf{r})\phi_j^*(\mathbf{r})[\hat{a}_i,\hat{a}_j] = \delta^3(\mathbf{r}-\mathbf{r}')\end{aligned} \tag{2.38}$$

where $\delta^3(\mathbf{r})$ is the three dimensional kronecker delta.

Applying Eq. 2.34 to Eq. 2.37 yields, for the kinetic part by using the commutation relations in Eq. 2.38,

$$\begin{aligned}\int d^3\mathbf{r}'\ \frac{\hbar^2}{2m}[\nabla'\hat{\Psi}^\dagger(\mathbf{r}')\nabla'\hat{\Psi}(\mathbf{r}'),\hat{\Psi}(\mathbf{r})] &= \frac{\hbar^2}{2m}\int d^3\mathbf{r}'\ \nabla'\hat{\Psi}^\dagger(\mathbf{r}')[\nabla'\hat{\Psi}(\mathbf{r}'),\hat{\Psi}(\mathbf{r})]+\\ &\qquad [\nabla'\hat{\Psi}^\dagger(\mathbf{r}'),\hat{\Psi}(\mathbf{r})]\nabla'\hat{\Psi}(\mathbf{r}')\\ &= 0 + \int d^3\mathbf{r}'\ \frac{\hbar^2}{2m}(-\nabla'\delta^3(\mathbf{r}'-\mathbf{r})\cdot\nabla'\hat{\Psi}(\mathbf{r}'))\\ &= \frac{\hbar^2}{2m}\nabla^2\hat{\Psi}(\mathbf{r}),\end{aligned} \tag{2.39}$$

where ∇' denotes derivatives with respect to the prime coordinates.

Hence, by continuing the process for the potential and the interaction term,

$$i\hbar\frac{\partial\hat{\Psi}}{\partial t} = \left(-\frac{\hbar^2}{2m}\nabla^2 + U(\mathbf{r})\right)\hat{\Psi}(\mathbf{r},t) + \int d^3\mathbf{r}\ \hat{\Psi}^\dagger(\mathbf{r}',t)V(\mathbf{r}-\mathbf{r}')\hat{\Psi}(\mathbf{r}',t)\hat{\Psi}(\mathbf{r},t). \tag{2.40}$$

At this point, mean field theory will be introduced to further simplify this relation. When the number of atoms in the condensate becomes quite large, than the $N_0 \pm 1 \approx N_0$. This

means that the operators $\hat{a}_i$ and $\hat{a}_i^\dagger$ behave like constants of value $\sqrt{N_0}$. Recall that the field operator is related to the operators by the relations in Eq. 2.33, so the field operator can be approximated by the expected value. More formally, the field operator of a BEC follows the relation

$$\hat{\Psi}(\mathbf{r},t) = \chi(\mathbf{r},t) + \hat{\Psi}'(\mathbf{r},t) \tag{2.41}$$

where $\chi(\mathbf{r},t) = \left\langle \hat{\Psi}(\mathbf{r},t) \right\rangle$ and $\hat{\Psi}'(\mathbf{r},t)$ is the small perturbation [2]. If most of the condensate is in the ground state, this small term can be neglected, leading the the substitution of χ for $\hat{\Psi}$.

Moreover, if the gas of atoms with a scattering length a is sufficiently diffuse, $(n|a|^3 \ll 1)$, then the three body interactions are negligible. Thus, the binary collisions can be characterized by the interaction potential $V(\mathbf{r}-\mathbf{r}') = g\delta^3(\mathbf{r}-\mathbf{r}')$, where for a 3D gas, $g = 4\pi\hbar^2 a/m$ [2, 20, 21]. Experimentally, this scattering length can be modified through the use of strong magnetic fields. This phenomenon is known as Feshbach resonance.

Thus, with these approximations in place, Eq. 2.40 becomes the GP equation

$$i\hbar\frac{\partial\chi}{\partial t} = \left(-\frac{\hbar^2}{2m}\nabla^2 + U(\mathbf{r}) + \frac{4\pi\hbar^2 a}{m}\left|\chi(\mathbf{r},t)\right|^2\right)\chi(\mathbf{r},t) \tag{2.42}$$

Expressing this wavefunction as $\chi = \chi_0 e^{-i\mu t/\hbar}$, the stationary state equation then becomes

$$\mu\chi_0(\mathbf{r}) = \left(-\frac{\hbar^2}{2m}\nabla^2 + U(\mathbf{r}) + \frac{4\pi\hbar^2 a}{m}\left|\chi_0(\mathbf{r},t)\right|^2\right)\chi_0(\mathbf{r},t) \tag{2.43}$$

Note that the wavefunction of the condensate $\chi(\mathbf{r},t)$ is the sum of all the individual particle wavefunctions, hence

$$\int d^3\mathbf{r}\ \left|\chi(\mathbf{r},t)\right|^2 = N, \tag{2.44}$$

with N being the number of particles.

2.3.3 Gross-Pitaevskii in Lower Dimensions

While condensation in lower dimensions is strictly impossible, due to the thermal fluctuations [2], in the limiting behavior of harmonic potential, quasi lower dimensional condensates can occur.

To illustrate this limit, consider the 3D harmonic potential, such as those created in magnetic traps with

$$V(\mathbf{r}) = \frac{1}{2}m\left(\omega_x^2 x^2 + \omega_y^2 x^2 + \omega_z^2 x^2\right), \tag{2.45}$$

where ω_j is the frequency of the trap in the j direction. Making the trap symmetric about the z-axis, so that $\omega_x = \omega_y = \omega_r$, then the limiting shapes of the atomic cloud can be described in terms of the ratio between the radial and axial frequency.

The cloud will be cigar-shaped if $\omega_z \ll \omega_r$ and pancake-shaped in the limit that $\omega_r \ll \omega_z$. Naturally, these correspond to the 1D and 2D limit respectively.

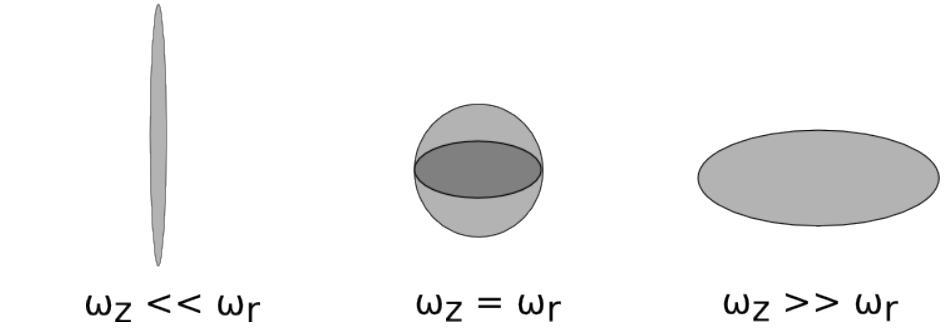

FIGURE 2.10: Depiction of the limits described in the text.

These relations can be understood through the solutions to the linear 1D Schrödinger equation with the simple harmonic potential ($V(x) = 1/2m\omega^2 x^2$). The solution wave function of this introductory quantum mechanical problem is proportional to $\exp\left(-m\omega x^2/2\hbar\right)$. Thus, the Full Width at Half Maximum is proportional to $1/\omega$, which means that larger frequencies corresponds to narrower probability densities.

While it seems reasonable to ignore the unused additional dimensions in our quasi-lower dimensional limits if such modes freeze out, this limiting behavior can be justified using the technique of separation of variables. Following the process of Carretero et al. [20], rewriting the condensate wavefunction as

$$\chi(\mathbf{r}) = \psi(z)\Phi(r) \tag{2.46}$$

with $r^2 = x^2 + y^2$. Here we define the radial part of the solution as

$$\Phi(r) = \Phi_0(r)e^{-i\gamma t/\hbar} \tag{2.47}$$

where $\Phi_0(r)$ is the ground state of the condensate in the radial component. Explicitly, this is

$$\Phi_0(r) = \left(\frac{m\omega_r}{\pi\hbar}\right)^{1/4} e^{-r^2 m\omega_r/2\hbar}. \tag{2.48}$$

For low enough temperatures, condensation occurs in a two step process. That is to say that for small enough T, where $T_{1D} < T_{3D}$ and $\hbar\omega_r < k_B T_{3D}$, the condensate does not have enough energy to be excited in the radial direction, but is not cold enough for condensation in all three dimensions [2]. Hence, we can focus on just one dimension as the radial wavefunciton must be in the ground state.

The ground state wavefunction in the radial direction solves the linear time dependent 2D Schrödinger equation

$$\gamma\Phi(r) = \frac{-\hbar^2}{2m}\nabla_r^2\Phi(r) + \frac{1}{2}\omega_r^2 r^2\Phi(r) \tag{2.49}$$

where the two dimensional laplacian $\nabla_r^2 = \frac{\partial^2}{\partial x^2} + \frac{\partial^2}{\partial y^2}$. As this approximation only depends upon the radial portion of the external potential, this potential will be redefined as $V(\mathbf{r}) = V(z) + (1/2)\omega_r^2 r^2$. So plugging in the separation of variables Eq. 2.46 wavefunction into the GP 2.42 yields

$$\Phi i\hbar\frac{\partial\psi}{\partial t} = -\Phi\frac{\hbar^2}{2m}\frac{\partial^2\psi}{\partial z^2} + \frac{1}{2}V(z)\psi\Phi + g|\Phi|^2|\psi|^2\Phi\psi \tag{2.50}$$

after using 2.49 to eliminate some terms. From this point, multiplying by Φ^* and integrating over all 2D space reduces above to the 1D GP

$$i\hbar\frac{\partial\psi(z)}{\partial t} = \left(-\frac{\hbar^2}{2m}\frac{\partial^2}{\partial z^2} + V(z) + g_{1D}|\psi(z)|^2\right)\psi(z) \tag{2.51}$$

where g_{1D} is defined as

$$g_{1D} = g\frac{\int\int|\Phi|^4\ r\ d\theta\ d\theta}{\int\int|\Phi|^2\ r\ d\theta\ d\theta} = g\left(\frac{m\omega_r}{2\pi\hbar}\right) = 2a\hbar\omega_r \tag{2.52}$$

Unfortunately, Eq. 2.51 is a nonlinear second order-differential equation with no general analytical solution. So to determine behavior of the BEC in this potential we must use approximation and numerical methods.

Chapter 3

Methods

3.1 Nondimensionalization

When working with theoretical models, nondimensionalizing the equations makes the algebra much simplier. In order to do this for the specific case of the atoms in a quasi-1D trap, first the external potential must be specified.

The anharmoinic potential is composed of two different sources: the linear gravitational potential and the exponentially decaying component from the EW. Mathematically, this is

$$V(z) = V_0 e^{-\kappa z} + m a_g z. \tag{3.1}$$

where a_g corresponds to the acceleration due to gravity; $V_0 = \Gamma\lambda^3 I_0/(8\pi^2 c\delta_3)$ is the maximum EW potential strength, Γ is the natural linewidth, λ is the resonance wavelength, I_0 is the EW peak intinsity, and δ_3 corresponds frequency detuning from resonance; while $1/\kappa = \Lambda/2 = \lambda_l/4\pi\sqrt{n^2\sin^2\theta - 1}$ where Λ is the EW decay length, with λ_l is the EW laser wavelength, n is the refractive index of the prism and θ is the angle of incidence [8, 16, 22]. Because the atoms will be thermalized if they hit the prism at the bottom of the GOST, the potential has the so called hard wall condition with $V(z \leq 0) = \infty$. Observe that this potential has a local minimum at $z_{min} = (1/\kappa)\ln(V_0\kappa/ma_g)$.

With this potential in mind, the 1D GP will be nondimensionalized by introducing a nondimensional space $\tilde{z} = \kappa z$ and time $\tau = t \times (mg)/(\hbar\kappa)$. Then to cancel the units of energy in the remaining terms, $\kappa/(ma_g)$ is multiplied to both sides of Eq. 2.51 yielding

$$i\frac{\partial}{\partial\tau}\tilde{\psi}(\tilde{z},\tau) = \left\{-\frac{k}{2}\frac{\partial^2}{\partial\tilde{z}^2} + \tilde{z} + \tilde{V}_0 e^{-\tilde{z}} + \tilde{G}|\tilde{\psi}(\tilde{z},\tau)|^2\right\}\tilde{\psi}(\tilde{z},\tau), \tag{3.2}$$

where $\tilde{\psi} = \psi/\sqrt{N}$ (to normalize the wavefunction to 1 rather than N), the kinetic energy constant $k = (\hbar^2\kappa^3)/(gm^2)$, $\tilde{G} = Ng(\kappa/ma_g) = 2Na\tilde{\omega_r}$ with the nondimensional radial frequency as $\tilde{\omega_r} = \hbar\kappa\omega_r/a_g m$, and then naturally, the dimensionless EW strength as $\tilde{V}_0 = \kappa V_0/a_g m$. Note that the z-axis frequency is $\omega_z = \sqrt{a_g\kappa}$ [8], so the nondimensional version is then $\tilde{\omega_z} = (\hbar/m)\sqrt{\kappa^3/a_g}$.

For ease of notation, from now on the tildes will be dropped.

3.2 Thomas-Fermi Limit

The GP equation is nonlinear, making analytical solutions impossible to find for any general potential. However, in the Thomas-Fermi limit (TF) where the BEC is cold enough and has a large enough number of atoms, the kinetic term is neglible compared to the interaction and potential terms. Specifically, the condition $Na\omega_z/\omega_r a_r \gg 1$ must be satisfied, where $a_r = \sqrt{\hbar/m\omega_r}$ [23]. Dropping this small kinetic term, leads to

$$|\psi| = \sqrt{\frac{1}{G}\left[\mu - V(z)\right]} \tag{3.3}$$

where μ is again the chemical potential. The function is assumed to go to zero outside the region where $\mu > V(z)$. The value of the chemical potential can be found from the normalization condition. This approximation is best closer to the center of the trap, as the edges have a larger curvature and likewise a larger kinetic energy component for these wavefunctions.

The hardwall condition constrains the wavefunction to the positive z-axis. Thus, the so called mirror image solution is used to enforce the boundary condition [24]. Analogous to method of image in electromagnetic problems, this method entails find a superposition between solutions of the form $\psi(z) = \psi_R(z) - \psi_L(z) = \psi_R(z) - \psi_R(-z)$, which naturally solves the boundary condition that $\psi(0) = 0$.

Foremost, the right hand solution ($\psi_R(z)$) will be found, and then from that point, the solution will be extended with more generality with the method of images.

3.2.1 Right Hand Solution

With the potential as $V(z) = z + V_0 e^{-z}$, then the normalization condition yields

$$1 = \frac{\mu}{G}\int_{z_1}^{z_2}\left(1 - \frac{z}{\mu} - \frac{V_0}{\mu}e^{-z}\right)dz \tag{3.4}$$

where z_1 and z_2 denote the zeros of the integrand. Because of the well shape of the potential and the condition that $\mu > V(z)$, then indeed there must be two zeros in the equation $\mu - V(z) = 0$. For small values of z, the exponential function dominates the linear function, thus $z_1 \approx \ln(V_0/\mu)$. Here the case of $V_0 > \mu$ is considered because in this case $z_1 > 0$. See section 3.2.2 for a more general approach. For large z, the decaying exponential vanishes, and so $z_2 \approx \mu$.

With these zeros, carrying out the integral yields,

$$G \approx \mu\Big([\mu - \mu/2] - [\log(V_0/\mu) + 1] \Big) \tag{3.5}$$

when neglecting the small terms $(V_0/\mu)e^{-\mu}$ and $\log(V_0/\mu)^2/(2\mu)$.

Simplifying,

$$0 = \mu^2 - \mu\left[\log\left(\frac{V_0}{\mu}\right) + 1\right] - 2G. \tag{3.6}$$

As this is a transendental equation, a complete solution cannot be found. However, because $G \sim 10^5$ and $V_0 \sim 10^3$ see section 4.1, then the term in the bracket is on the order of 1. Thus, the squared term will dominate. So to an acuracy of better than few percent,

$$\mu \approx \sqrt{2G}. \tag{3.7}$$

This can be seen by order of magnitude anaylsis. Even if $G = 10^4$, which would be quite low, then

$$\mu^2 \sim 2 \times 10^4 \gg \mu\left[\log\left(\frac{V_0}{\mu}\right) + 1\right] \approx 10^2,$$

which confirms the small percentile error.

Therefore, the right handed solution is then

$$\psi_R(z) = \sqrt{\left(\frac{\mu}{G}\right)\left(1 - \frac{z}{\mu} - \frac{V_0}{\mu}e^{-z}\right)} \tag{3.8}$$

Indeed using a algebraic integrator for Eq. 3.8 from z_1 to z_2, the result is

$$\int_{z_1}^{z_2} \psi_R(z)dz = 1 - \sqrt{\frac{2}{G}} + V_0\frac{e^{-\sqrt{2G}}}{G} + \frac{\log 2 - 2\log(V_0/\sqrt{G})}{\sqrt{2G}} + \frac{(\log(V_0/\sqrt{2G})^2}{2G}, \quad (3.9)$$

which indeed approaches 1 for large G.

3.2.2 More General Approximation

In the previous section, $V_0 > \mu$. This simplified the process because the wavefunction automatically satisfied the hardwall condition because $z_1 > 0$. This is not true of $V_0 < \mu$, which occurs if there are quite a large number of atoms $N \sim 10^6$.

To generalize Eq. 3.8, the left hand solution is introduced as $\psi_L(z) = \psi_R(-z)$. Defining the total wavefunction as a linear combination of the right and left hand solution, then

$$\psi(z) \propto \psi_R(z) - \psi_L(z), \quad (3.10)$$

where it is not strictly equal because of the possble normalization concerns in the region where the two hands of the solution overlap, see Fig. 3.1. Although this constant is important for quantitative analysis, qualitatively the behavior of the wavefunction should remain the same.

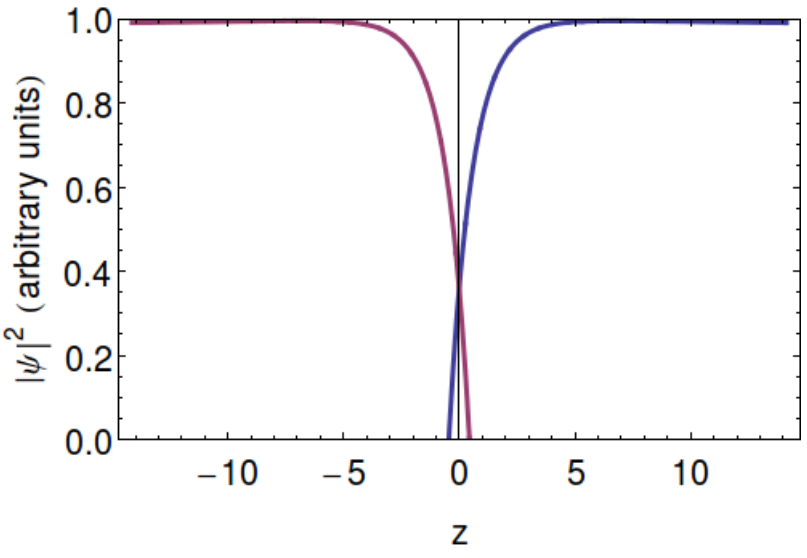

FIGURE 3.1: The left and the right handed solutions interfer with each other in between a specific region. This will affect the overall wavefunction's normalization, although the effect is quite small.

If $V_0 < \mu$, then $\log(V_0/\mu) < 0$. Defining ξ as

$$\xi = \frac{1}{2}\left|\log\left(\frac{V_0}{\sqrt{2G}}\right)\right| + \frac{1}{2}\log\left(\frac{V_0}{\sqrt{2G}}\right), \tag{3.11}$$

so that $\xi = 0$ if $V_0 < \mu$ when there is overlapping and $\xi = \left|\log\left(V_0/\sqrt{2G}\right)\right|$ in the case that $V_0 > \mu$ as was the case in the previous section.

In the former case, with the interference, some of the right hand solution spills into the other side of the wall, so the normalization constant must be altered.

Since, the wavefunction quickly approaches zero around the overlap of the solutions, the intergral of the probability density. is negligible for $0 < z < \xi$. Thus, to have a normalized solution, the probability density of this cut-off region should be subtracted from the orignal constant. Naming this integral $M_{\text{cut off}}$, the change in the normalization constant is found to be

$$M_{\text{cut off}} = \int_{\log(V_0/\mu)}^{-\log(V_0/\mu)} \left(1 - \frac{z}{\mu} - \frac{V_0}{\mu}e^{-z}\right) dz \tag{3.12}$$

$$= -2\log\left(\frac{V_0}{\mu}\right) - 1 + \left(\frac{V_0}{\mu}\right)^2 \tag{3.13}$$

And so, the new normalization constant, M, is written as

$$M = \begin{cases} \sqrt{\mu/G - |M_{\text{cut off}}|} & \text{for } \xi = 0 \\ \sqrt{\mu/G} & \text{for } \xi \neq 0 \end{cases} \tag{3.14}$$

Often for a reasonable number of atoms, $M_{\text{cut off}}$ will be quite small because in this case $V_0 < \mu$, so the ratio $V_0/\mu \leq 1$ making both the log term and the sqared term small.

For completeness, this leads to

$$\Psi(z) = \begin{cases} M\left[\sqrt{\left(1 - \frac{z}{\mu} - \frac{V_0}{\mu}e^{-z}\right)} - \sqrt{\left(1 + \frac{z}{\mu} - \frac{V_0}{\mu}e^{+z}\right)}\right] & \text{for } \xi < z < \left|\log\left(\frac{V_0}{\sqrt{2G}}\right)\right| \\ M\left[\sqrt{\left(1 - \frac{z}{\mu} - \frac{V_0}{\mu}e^{-z}\right)}\right] & \text{for } \left|\log\left(\frac{V_0}{\sqrt{2G}}\right)\right| < z < \mu, \end{cases} \tag{3.15}$$

Note how for $\xi \neq 0$, not only the constant outfront, but the entire function itself reduces down to the original right hand solution.

3.3 Split-Step Method

In addition to appropriate approximations, the more brute force option is using numerical techniques. Based on the techniques developed by Javanainen and Ruostekoski [25], the time dependent wavefunction is propagated forward in time using the method known as split-step. However, this method can also be used to find the ground state of the wavefunction in a certain external potential by propagating it in imaginary time, see Subsection 3.3.1.

In general, the propagation of a state later in time can be found by $\psi(z,t) = e^{-i\hat{H}t/\hbar}\psi(z,0)$, where $e^{-i\hat{H}t/\hbar}$ is an unitary operator called the time-evolution operator. Unfortunately, even for the linear Schrödinger equation, the kinetic and potential operators do not commute. This makes the propagation of the wavefunction difficult to calculate because $exp(-i(\hat{T}+\hat{V})t/\hbar) \neq exp(-i\hat{T}t/\hbar)exp(-i\hat{V}t/\hbar)$. However, if they did commute, then the wavefunction (with units) at a time step later would be easily found by multiplying the initial wavefunction by $e^{-ip^2t/2\hbar m}$ in momentum space and then multiplying this by $e^{-i\hat{V}(z)t/\hbar}$ in position space.

Thus, to overcome this difficulty, the split-step operator method uses properties of linear algebra to find an approximate solution that allows one to split up the propagation operator. In essence, a solution of the form

$$e^{\lambda(\hat{A}+\hat{B})} = e^{\lambda\beta_n\hat{B}}e^{\lambda\alpha_n\hat{A}}\dots e^{\lambda\beta_1\hat{B}}e^{\lambda\alpha_1\hat{A}} + O(\lambda^m) \tag{3.16}$$

is sought with the order of the error m to be as large as possible [25]. To find the coefficients, one expands out the exponentials in a taylor series and then matches the terms coefficients on both sides of the equation. For example, expanding the time propagator for the linear Schrödinger equation, dropping all third or higher order terms yields,

$$e^{\lambda(\hat{T}+\hat{V})} \approx 1 + \lambda(\hat{T}+\hat{V}) + \lambda^2(\hat{V}^2/2 + \hat{V}\hat{T} + [\hat{T},\hat{V}]/2 + \hat{T}^2), \tag{3.17}$$

where $[\hat{T},\hat{V}]$ is again the communtator relation of the kinetic and the potential operator. Similarly, expanding out the right side of Eq. 3.16, yields

$$
\begin{aligned}
&e^{\lambda\beta_2\hat{V}}e^{\lambda\alpha_2\hat{T}}e^{\lambda\beta_1\hat{V}}e^{\lambda\alpha_1\hat{T}} \approx \\
&\quad (1+\lambda\beta_2\hat{V}+\frac{\lambda^2}{2}\beta_2^2\hat{V}^2+\dots)(1+\lambda\alpha_2\hat{T}+\frac{\lambda^2}{2}\alpha_2^2\hat{T}^2+\dots)\times \\
&\quad (1+\lambda\beta_1\hat{V}+\frac{\lambda^2}{2}\beta_1^2\hat{V}^2+\dots)(1+\lambda\alpha_1\hat{T}+\frac{\lambda^2}{2}\alpha_1^2\hat{T}^2+\dots)
\end{aligned} \tag{3.18}
$$

After expanding out the terms, best done with a symbolic manipulator software such as *Mathematica*, and matching the terms, the system of equations is found to be

$$
\left.\begin{aligned}
\alpha_1+\alpha_2 &= 1 \\
\beta_1+\beta_2 &= 1
\end{aligned}\right\}\text{From } \lambda \text{ terms}
$$

$$
\left.\begin{aligned}
\alpha_2\beta_1 &= 1/2 \\
\alpha_1\beta_1+\alpha_1\beta_2+\alpha_2\beta_1+\alpha_2\beta_2 &= 1 \\
\beta_1\beta_2+\beta_1^2/2+\beta_2^2/2 &= 1/2 \\
\alpha_1\alpha_2+\alpha_1^2/2+\alpha_2^2/2 &= 1/2
\end{aligned}\right\}\text{From } \lambda^2 \text{ terms} \tag{3.19}
$$

There exists two possible solutions to this, namely $\alpha_1 = \alpha_2 = 1/2$ with $\beta_1 = 1$ and the other is $\beta_1 = \beta_2 = 1/2$ with $\alpha_2 = 1$ [25]. With this in mind, the propagation factor has been separated so that it can be easily propagated alternating in position, momentum, and then position space again for the first solution, corresponding to the factor $\exp(-i\delta\tau\hat{T}/2)\exp(-i\delta\tau\hat{V})\exp(-i\delta\tau\hat{T}/2)$ for a small time step $\delta\tau$.

The transition from the Schrödinger to the GP involves the additional interaction term. This term's dependence on ψ begs the question of which ψ, is it the original wavefunction or the wavefunction after one small step in momentum space? After thorough investigation, Javanainen and Ruostekoski found that to an error of $O(\delta\tau^3)$ the final wavefunction using the following procedure [25].

$$
\begin{aligned}
\psi_0 &= \psi(z,\tau) \\
\psi_1 &= \exp(-i\delta\tau\hat{T}/2)\psi_0 \\
\psi_2 &= \exp(-i\delta\tau(\hat{V}+|\psi_1|^2)\psi_1 \\
\psi(z,\tau+\delta\tau) &= \exp(-i\delta\tau\hat{T}/2)\psi_2.
\end{aligned} \tag{3.20}
$$

In this way, each successive step relies only on the previous. ψ_1 and $\psi(z,\tau+\delta\tau)$ are best evaluated in momentum space, so it will be necessary to apply Fourier transformations when calculating the propagation of the wavefunction.

3.3.1 Propagation in Imaginary Time

Not only can this split-step method be applied to find the evolution of the wavefunction, it can also be used to find the ground state of a give potential. This can be done by propagating in imaginary time defined by $\zeta = i\tau$. When one does this, the time-evolution operator becomes a decaying exponential with the higer energy states decaying more rapidly. To avoid the whole function decaying down to zero, the wavefunction will be renormalized after each time step. Simply, the constant out front will be numerically found by integrating the wavefunction over its range. Additionally, note that the above process requires an initial function ψ_0. In this work, a trial guassian curve was found to work well.

In more detail, this method works based on the fact the wavefunction can be written in terms of its eigenstates ϕ_j, each with energy E_j. Thus,

$$\psi(z,\tau) = e^{-\zeta\hat{H}/\hbar}\psi(z,0) = \sum_j e^{-\zeta\hat{H}/\hbar}\phi_j(z) = \sum_j e^{-\zeta E_j/\hbar}\phi_j(z) \tag{3.21}$$

For any wavefunction, the energy of the ground state is lower than the energy of all the other states, ie $E_j > E_0$ for all $j \neq 0$. Thus after a substantial amount of imaginary time, the higher energy states will exponentially decay faster than the ground state. Clearly, the larger the time the better, but plotting the energy over imaginary time shows when this leveling off occurs.An example of such a plot is seen in Fig. 3.2. Note that the energy E is found by

$$E = \int \mathrm{d}z \left[\frac{k}{2}\left|\frac{\partial\psi}{\partial z}\right|^2 + V(z)\left|\psi\right|^2 + \frac{G}{2}\left|\psi\right|^4\right], \tag{3.22}$$

note the factor of $1/2$ in the interaction term coming from the careful treatment of the condensate wavefunction [2, 21].

3.3.2 Harmonic Potential Example

To illustrate this method, consider the simple harmonic potential $V(z) = (1/2)m\omega_z^2 z^2$. The TF limit would suggest that with a nondimensional version of the potential $V(z) = \beta^2 z^2$, that the wavefunction density would be given by

$$|\psi|^2 = \frac{1}{G}\left[\left(\frac{3}{4}\beta G\right)^{2/3} - \beta^2 z^2\right] \tag{3.23}$$

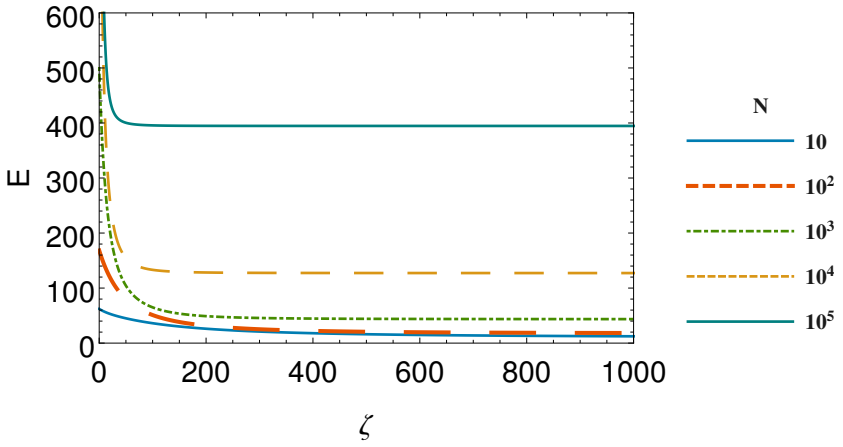

FIGURE 3.2: Energy of the BEC as a function of imaginary time for various number of atoms. The exponential decay of the higher energy eigenstates quickly reduces the higher energy states.

Indeed, using the same nondimensional scheme as before with $\beta = 5$ and using a value of $N = 10^3$ so that the TF approximation approaches the numerical behavior, see Fig. 3.3. Note how the kinetic energy expands the cloud, so the numerical solution is wider than the TF approximation. This error will decrease for larger values of N, where the interaction term becomes even more dominant. The convergence of the numerics in imaginary time can be seen in Fig. 3.4.

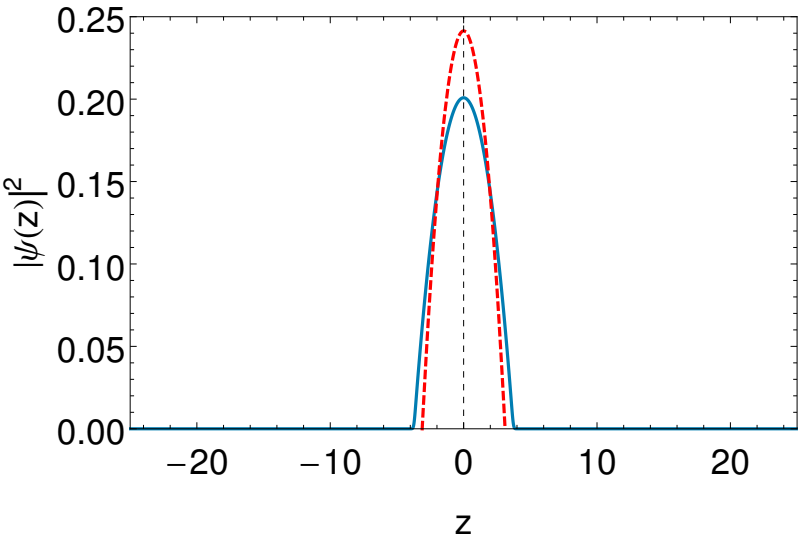

FIGURE 3.3: Shown is a comparison between the numeric and the TF results for a simple harmonic oscillator, with $\beta = 5$ and $N = 10^3$. The dotted curve is the TF approximation, which is clear from its behavior at the boundary where it is more narrow.

See Appendix A for the code that finds this ground state.

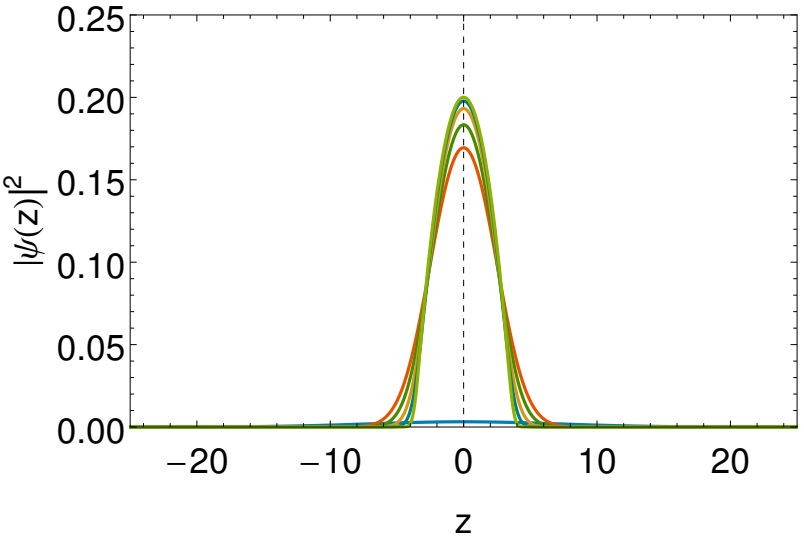

FIGURE 3.4: Shown is the evolution of the wavefunction in imaginary time at different time steps. It very quickly converges from a wide gaussian initial guess to the parabola solution.

Chapter 4

Results

4.1 Parameter Values

While there are to my knowledge no present literature on experiments done in the 1D limit, the Universität Innsbruck experiments on 2D surface traps provide reasonable parameters to be used here [8].

Based on this work, the parameters selected will be as follows. The star notation here will denote those terms with dimensions to avoid confusion. For the inverse decay length, $\kappa = 2/\Lambda = 1.43 \times 10^6$ m^{-1}, where $\Lambda \approx 1.4\mu$m. Thus, because the axial frequency $\omega_z^* = \sqrt{\kappa a_g}$, the value is then $\omega_z^* \approx 2\pi \times 600$ Hz. The strength of the EW is about $V_0^*/k_B \approx 100$ μK, where k_B is the Boltzmann constant. To satisfy the condition $\omega_z^* \ll \omega_r^*$, the radial frequency is assumed to be $\omega_r^* = 100\omega_z^* = 2\pi \times 60$ kHz. Further, for a specific interaction energy, the s-wave scattering wavelength is repulsive ($a^* > 0$) and give by $a^* = 440$ a$_0$ with the Bohr radius a_0. Note that this is at a magnetic field of 26.8 Gauss.

With these parameters in mind, now the nondimensional scales will be specified. Foremost, the characteristic energy scale is given by $a_g m/\kappa = 1.52 \times 10^{-30}$J $= 8.99 \times 10^{-12}$eV while the time scale is given by $(\hbar\kappa)/(ma_g) = 69.2$ μs, so this means $\tau = 20$ corresponds to 1.38 ms.

Lastly given the energy and time scales, the nondimensional constants will be explicitly written out term by term in GP. First, the constant in kinetic term is given by $k = (\hbar^2\kappa^3)/(a_g m^2) = 0.067$, where the factor of κ^2 comes from the derivative. Next, the nondimensional maximum of the potential is given by $V_0 = \kappa V_0^*/(a_g m) = 906$.

To specify the interaction strength, the nondimensional scattering length is scaled as $a = a^*\kappa = 0.0333$ and the nondimensional radial frequency is given by $\omega_r = \hbar\kappa\omega_r^*/(a_g m) = 26.1$,

while this makes the nondimensional axial frequency $\omega_z = 0.261$. Thus, the interaction strength constant is then given by $G = 2Na\omega_r = 1.73N$, so G is about the number of atoms in this nondimensional scheme.

In the following subsections, parameter space will be explored mostly by altering the range of the number of atoms from 10^2 to 10^6. Indeed, with these values, both the potential term and interaction terms do dominate the kinetic term, so the TF approximation should apply.

4.2 Comparison of Split-Step and TF

Because the shape of the potential is anharmonic, given by Fig. 4.1, the wavefunciton should resemble a gaussian curve for very small values of N. As the interaction energy increases the atoms begin to be pushed away from each other due to the positive scattering lengths considered here. However, as the atoms approach the hardwall, they can no longer expand in that direction. Hence, the probability density will begin to become less and less symetric, see Fig. 4.2.

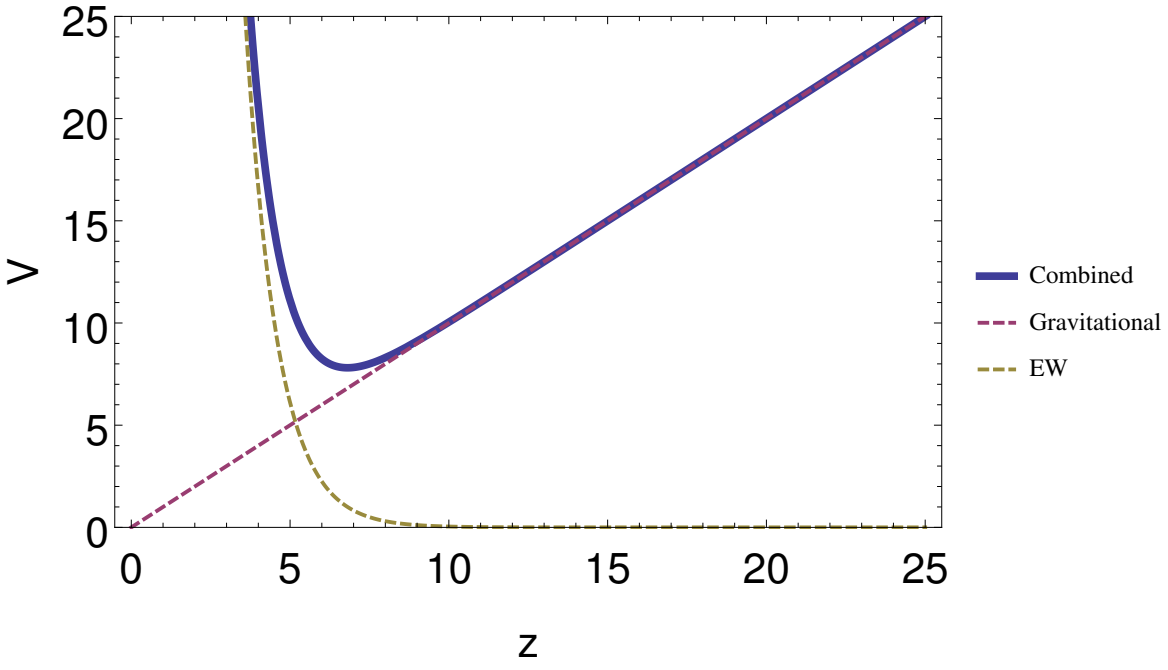

FIGURE 4.1: Plot of the components of the anharmonic potential as well as the total potential function given by the solid curve.

Note how the peak of the probability density does not move significantly. This behavior is reasonable as it most of the atoms should reside in the well's minimum which corresponds to $z_{\min} = 1 + \log(V_0) = 7.8$. Further, note how in the limit of small G and large V_0, GP

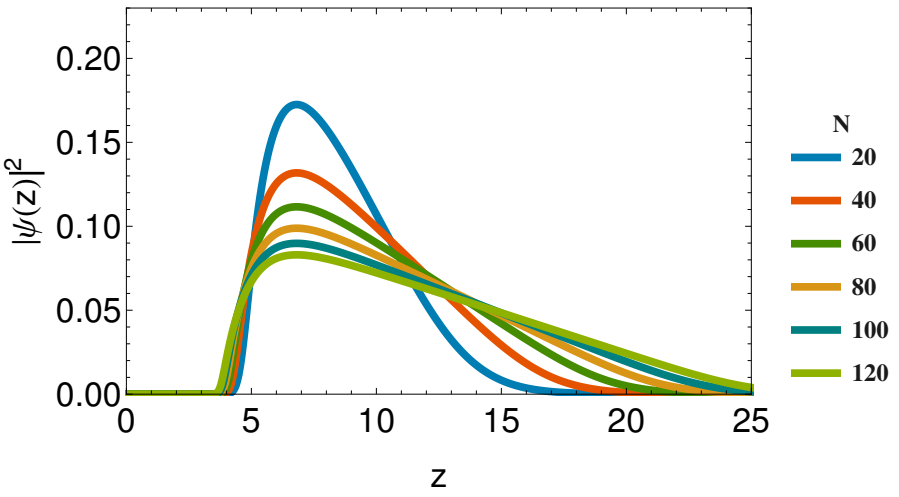

FIGURE 4.2: Probability density plots from the numerical calculations for various values of N. Note the transistion to from the Airy function solution to the triangular solution.

equation reduces to Schödinger's equation with the potential $V(z) = z$. The solution to this is an Airy function [26], which indeed has the form similar to that give by the blue curve in Fig 4.2. Thus, the numerical results here behaves appropriately in the limit of small N.

As the number of atoms increases, the TF approximation becomes more accurate. This function, see Eq. 3.15, has a triangular-like shape resulting from the exponential dominating for small z and the linear function dominating for large z. The agreement between these two methods is quite remarkable see Fig. 4.3 and 4.4. Naturally, the percent error decreases for larger number of atoms, but it is surprising to get a max percentage error of around 15 % even for just 10 atoms! This is most likely due to small size of the kinetic energy compared to the potential term. Further, the plots of percent error match expectations, as the error is larger near the turn off points, where the kinetic energy plays a more prominant role.

4.3 Exploring Parameter Space

With this model in place, it is important to relate back to possible experimental results by exploring parameter space. The mean position will be found in the regular manner of $\langle z \rangle = \int z|\psi|^2 \mathrm{d}z$. Because the probability density is triangular in shape, the width of the cloud is not as well defined. For this purpose, the standard deviation $\sigma = \sqrt{\langle z^2 \rangle - \langle z \rangle^2}$ will be used as a measure of width, as wider curves will indeed have a larger standard

deviation. The numerical results will be used to calculate the mean position and width, as the agreement between the numerics and analytical approximation is quite good.

If the laser intensity is increased in the EW beam, then V_0 will increase. Effectively, this shifts the minimum of the well farther away from the wall, so the mean position of the atoms should increase, as shown in Fig. 4.5. For reference, $z = 1.43$ corresponds to 1 μm. Note that the larger number of atoms has a slightly greater mean position. Again this is caused by the fact the atoms cannot extend into the hardwall, so with more atoms, they must be pushed farther outwards.

However, the change in V_0 does not significantly affect the width of the cloud. Effectively, it only shifts the position by extending the hardwall. On the other hand, because the atom-atom interaction strength is directly proportional to the number of atoms in the trap, the width is highly dependent on N. For smaller N, the width is rather small and constant, but suddenly increases quite rapidly for larger N see Fig. 4.6.

4.4 Time of Flight Expansion

Time of Flight (TOF) expansion is a standard technique in BEC experiments where data is collected by suddenly turning off the trapping lasers or magnetic fields. Images of the cloud are taken by exciting atoms with a probe beam, which will destroy the cloud. Comparisions of these images collected over numerous runs at different times in the expansion determines properties such as kinetic energy of the cloud.

Although the BEC GOST experiment done by the Universität Innsbruck group is two dimensional, they retained their radial confining beams when measuring the remaining number of atoms in the trap after a vertical TOF expansion [8]. Thus, in this case with $N = 2400$ atoms, $V_0^*/k_B = 50$ μK and $\omega_r^* = 20\pi$, the quasi-1D model developed here should apply.

To simulate this expansion, the wavefunction was propagated forward in real time with the EW portion of the potential turned off. The expansion times are short enough, that the atom-atom interaction is presumed to be negligible because the atoms are not likely to collide during these time scales. If the atoms touch the prism they are lost to thermalization. So to determine the remaining number of atoms, the wavefunction is propagated numerically forward in time without the hardwall condition, and then the remaining number of atoms will be determined by $\int_0^\infty |\Psi(z,\tau)|^2 dz$, as the probability that the wavefunction extends past $z = 0$ corresponds to the thermalization of that proportion of atoms. The agreement between numerics (the solid curve) and the experimental results (the circle dots) is quite good, see Fig. 4.7.

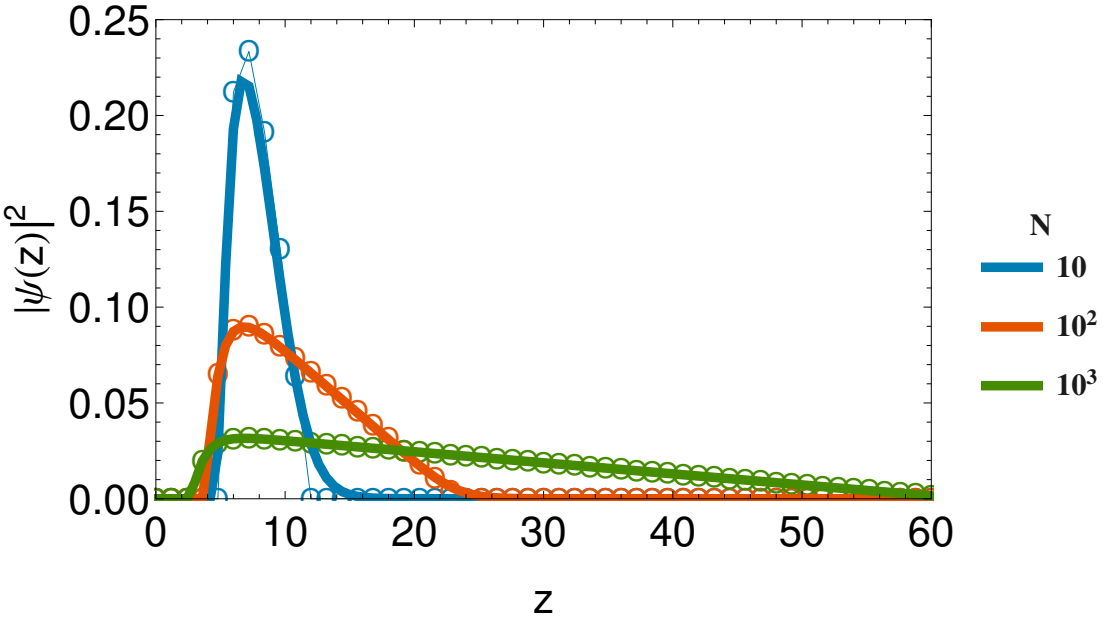

(A)

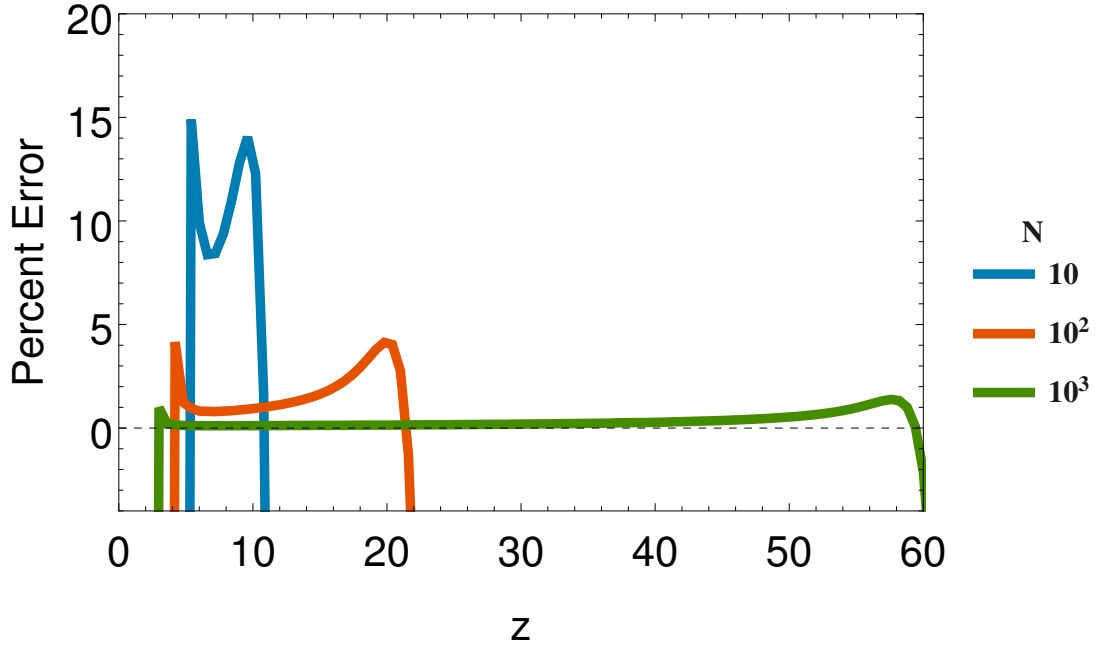

(B)

FIGURE 4.3: (A) Comparison of the the split-step numerical calclulation (solid lines) and the TF approximation (circular points) for small N. (B) The percent error here is $(|\psi_{\mathrm{TF}}|^2 - |\psi_{\mathrm{num}}|^2)/|\psi_{\mathrm{num}}|^2 * 100$. Note that past the range of validity, the TF probability density goes to zero, so the percent error approaches -1 at this z coordinate.

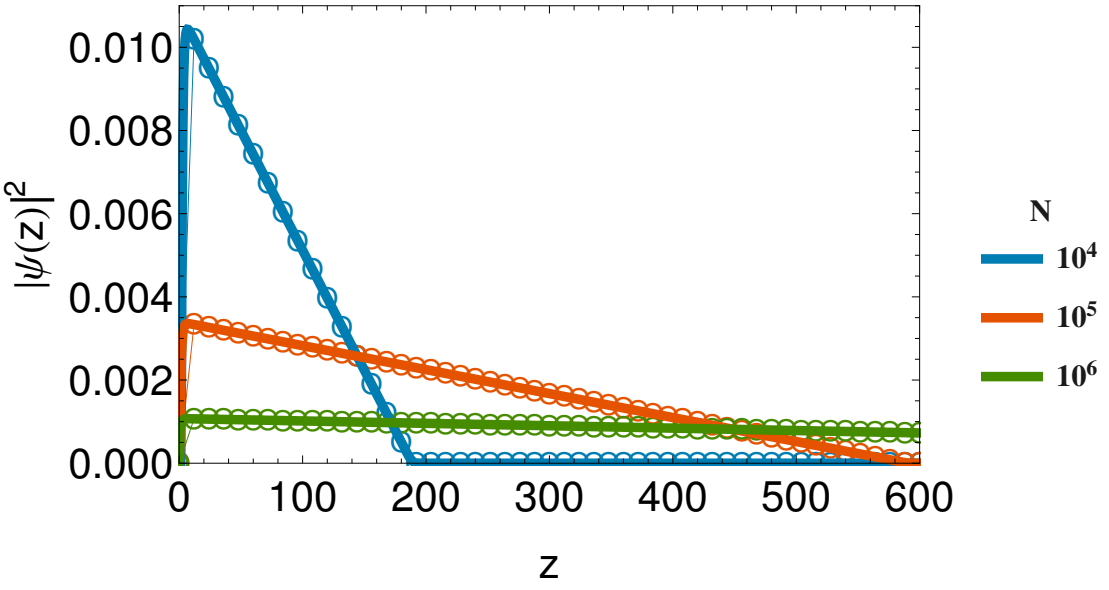

(A)

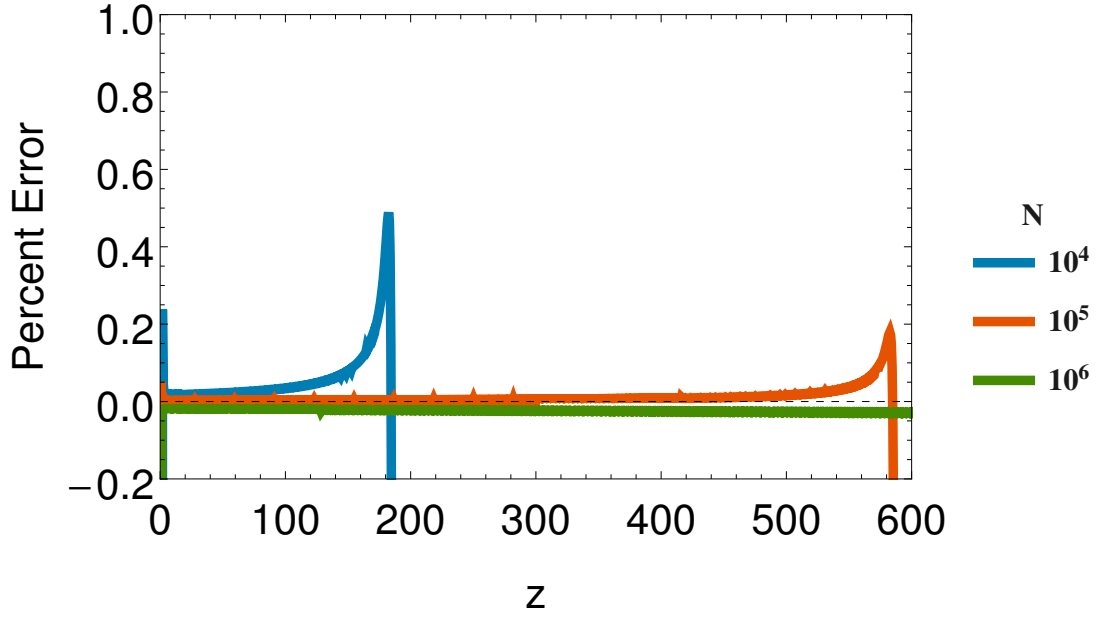

(B)

FIGURE 4.4: (A) Comparison of the the split-step numerical calclulation (solid lines) and the TF approximation (circular points) for large N. (B) The percent error here is $(|\psi_{\text{TF}}|^2 - |\psi_{\text{num}}|^2)/|\psi_{\text{num}}|^2 * 100$. Note that past the range of validity, the TF probability density goes to zero, so the percent error approaches -1 at this z coordinate. The agreement is remarkable for large N.

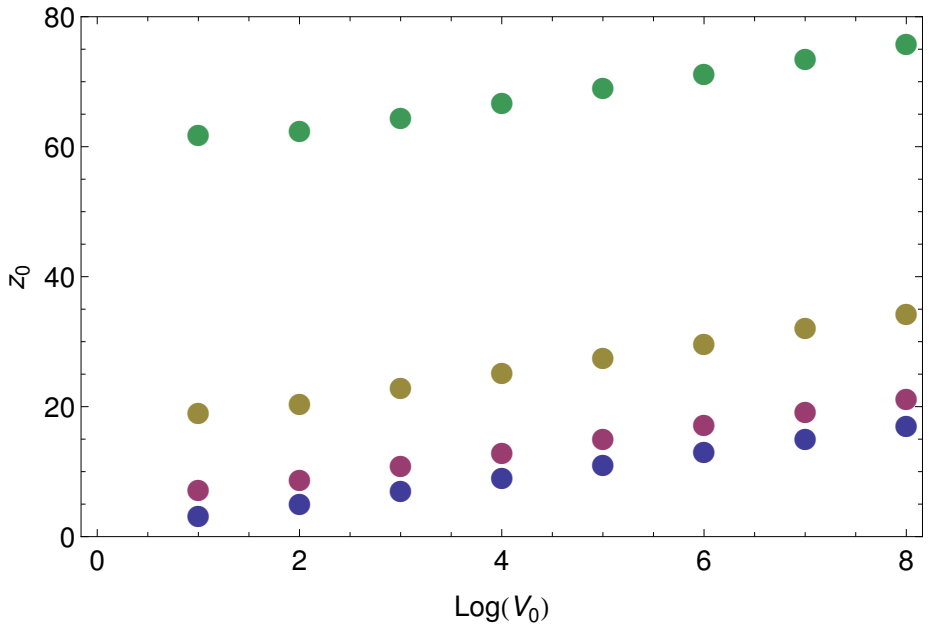

FIGURE 4.5: Increasing the intensity of the EW laser beam increases the constant V_0. From the numerical calculations, such an increase causes the mean position of the atomic cloud to be extended outwards. However these shifts are rather small for large increases in V_0, note the $\log_{10}$ scale. The different color dots (purple, magenta, gold and green), corresponds to $N = 10$, 10^2, 10^3, and 10^4 respectively.

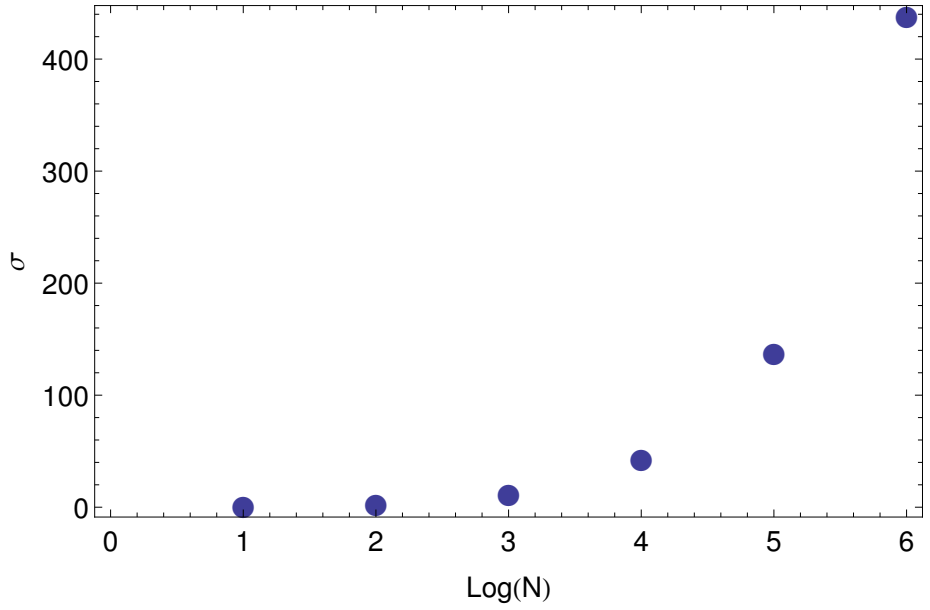

FIGURE 4.6: For a constant $V_0 = 906$, the effect of the atom-atom interaction on the standard deviation is shown. Note that the atom-atom interaction is directly proportional to the number of atoms. On this plot the $\log_{10}$ is used for the x-axis.

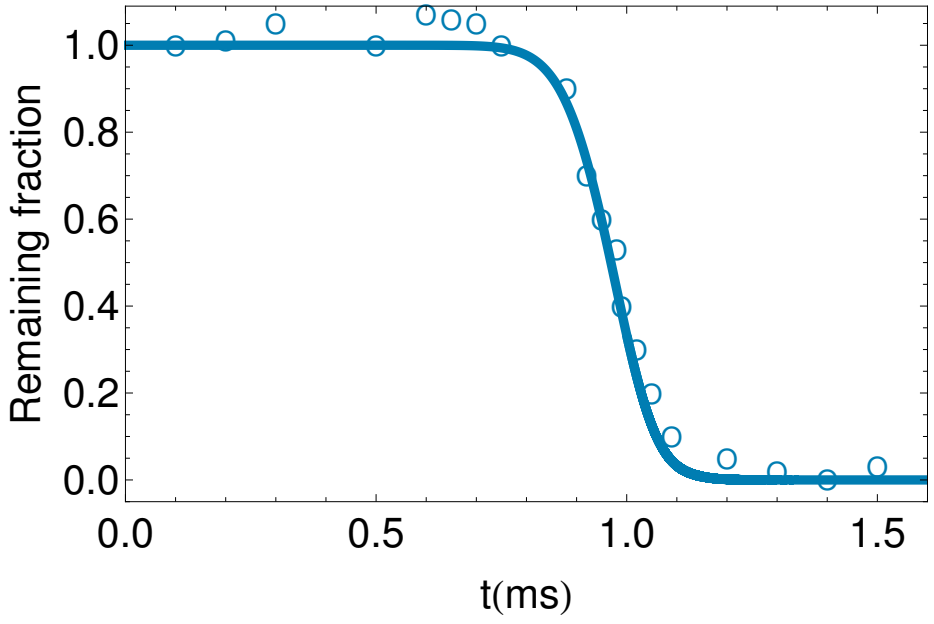

FIGURE 4.7: The fraction of remaining atoms during time of flight in a vertical expansion. Here empty circles reproduced from the Innsbruck experimental result [8] and solid line shows the numerical results, with real time on the x-axis. The error bars on the data points are less than or equal to the size of the circle used to plot the data.

Chapter 5

Conclusion

5.1 Overview of results

In this work, the behaivor of atoms in a quasi-1D GOST is investigated. In such a trap, the atoms are initially cooled down using a MOT. Then they are transfered to a GOST, which consists of an exponentially decaying EW dipole force to compensate for the downwards pull of gravity. This leads to an anharmonic potential along the z-axis. A hollow laser beam is used to contain these atoms radially, and for this work is assumed to be tightly confining such that the motion of the atoms is essetinally only along the z-axis. In recent experiments at the Universität Innsbruck group in Austria [8], an electric dipole trap evaporative cools the atoms down to a low enough temperature for condensation to occur in the GOST.

To model such a system, the GP equation is derived from first principle using quantum field theory and mean field approximation. The atom-atom interaction's strength increases with larger numbers of atoms, and is modeled by extremely decaying potential strengths approximated by a dirac delta function.

Due to the nonlinear nature of the GP, it cannot be solved analytically for an arbitrary potential. However, for large N, the kinetic energy is quite small compared to the potential and atom-atom interactions, making the Thomas-Fermi approximation suitable. In this scheme, the kinetic term is dropped and the chemical energy is found by satisfying the normalization condition. In addition, numerical study of these wavefunctions have been done via the split-step method.

The two different methods agree quite well. From these models, it is clear that the hardwall condition forces the atoms to form a triangular-shaped probability density with its peak at the minimum of the potential. Stronger EW lasers, corresponding to a

higher V_0, shifts the position of the probability density in space, while larger populations of atoms expands the width of the cloud.

Further, the results of this simulation agree quite well with the vertical TOF expansion of the Innsbruck group, where they kept the radial confinement but allowed the atoms free expansion along the z-axis.

5.2 Future Outlook

To better match experimental results, it would be interesting to extend this work for 2D systems. If accomplished, then the vertical and radially contained energy states of the system could be determined, and their energy could be compared with existing experimental results [22].

It would also interesting to look at the possibility of an attractive interatomic potential, such as the one of ^{7}Li. This would entail an $a < 0$. The stability of such systems is often a concern.

Lastly, the techniques developed here can be applied to other potentials as well. An interesting application would be examining the interaction between two expanding clouds from different potential wells. This would be particularly interesting for lower dimensional BECs.

Appendix A

Propagation in Imaginary Time

Matlab code for the propagation in imaginary time of the simple harmonic example calculation.

```
 %clear everything
clc
clf
clear all

%for nondimensionalization
kin = 0.0669923 ; %kinetic energy constant.

%~~~~~~~~~~~~~~~Initialize Space~~~~~~~~~~~~~~~~~~~~~~~

Lx=30; %length of x
Nx=10000; %number of x data points
dx=2*Lx/Nx;
x=(-Lx:dx:Lx-2*Lx/Nx);% x coordinate
kx=pi*[0:Nx/2 -Nx/2+1:-1]/(Lx);% wave vector
k2xm=kx.^2;  %wave vector squared

%~~~~~~~~~~~~~~Initialize Time~~~~~~~~~~~~~~~~~~~~~~~~~~
tf=0.1; %total time
dt=0.001; %time step
Nt=tf/dt;% number of time slices

%%%~~~~~~~~~~~~~~~~~~~~~~~~Setting up Potential~~~~~~~~~
```

```
beta= 5; %amplitude of softwall exponential term
Gconst = 1.73486 %constant without the number of atoms
NumAtoms = 10^3
G= NumAtoms * Gconst;  %interaction term

%Potential itself
V= beta^2 * x.^2;

%~~~~~~~~~~~~~~~~~original guess~~~~~~~~~~~~
%~~~sometimes a better guess is needed to avoid numerical error
eps = 100;
u=(1/sqrt(pi*eps))*exp((-.5/eps)*(x.^2)) ;
u0 = u;

%~~~~~~~~~~~~initializing stuff solving loop~~~~~~~~~~~~
pot=0; E=0; Mu=0; Ur=0; T=0; m=1;


%split opperator method~~~~~~~~~~~~~~~~~~~~~~~~~~~~~~~~~~

for n=0:Nt-1                            %so there are Nt loops
    v=fft(u);                           %fft is fourier transform
    vna=exp(-0.25*kin*dt.*(k2xm)).*v;
    una=ifft(vna);
    pot=V + (G)*(abs(una).^2);
    unb=exp(-1*dt*pot).*una;
    vnb=fft(unb);
    v=exp(-0.25*kin*dt.*(k2xm)).*vnb;
    u=ifft(v);

    % must renormalize the function
    intv=sum(u(:).^2)*dx;
    u=(u)./sqrt(intv);

    if(mod(n-1,10)==0) %Probability Density for various intermediate steps
        figure(1); clf;

        h= plot(x,abs(u).^2);
        set(h(1),'LineWidth',2);
```

```
    camlight right; lighting phong  %makes the video smooth
    xlim([-Lx Lx])                  %axes
    drawnow;
end

% The if statements are used for ploting various time steps later on
if(n==1)
    u1 = u;

elseif(n==2)
    u2 = u;

elseif(n==4)
    u4 = u;

elseif(n==8)
    u8 = u;

elseif(n==20)
    u20 = u;

end

%energy
dk=dx/(Nx);
Kn=sum( abs(k2xm.*fft(u).^2)  )*kin*dk/2; %total kinetic energy
E1=V.*u.^2+(G/2)*abs(u).^4;
E2=sum(E1)*dx;
E(m)=real(Kn+E2);
E5(m,1)=m;
E5(m,2)=E(m); %storing calculated values

%chemical potential
MKn= Kn;
Mu1=V.*u.^2+(G)*abs(u).^4;
Mu(m)=real(MKn+sum(Mu1(:)).*dx);

%make the Time matrix
```

```
    T(m)=n;

    %next step in E, Mu, T
    m=m+1;
end



%Energy over time to show convergence
figure(2);
scatter(T,E,40,'MarkerEdgeColor','b',...
             'MarkerFaceColor','c',...
             'LineWidth',1.5)

%Plot of the converging probability density
figure(3)
plot(x, u0.^2, x, u1.^2 , x,u2.^2 , ...
    x, abs(u4).^2, x, abs(u8).^2, x, abs(u20).^2)
xlabel('$z$','Interpreter', 'LaTex')
ylabel('$|\psi|^2$', 'Interpreter', 'LaTex')

% exporting data
name1 = 'wavefun.dat';
dlmwrite(name1, u, 'delimiter', '\t')

ugrand = [u0; u1; u2; u4; u8; u20];
for j = 1:6
    name2 = sprintf('wavefunpart_%d.dat', j);
    dlmwrite(name2, ugrand(j,:), 'delimiter', '\t')

end

name3 = 'x.dat';
dlmwrite(name3, x, 'delimiter', '\t')
```

Appendix B

Time of Flight Expansion

The code for time of flight expansion is below. The ground state is first found by propagating the wavefunction in imaginary time, and then it is propagated in real time to find the remaining fraction. The atoms that pass $z = 0$ are assumed to be lost due to thermalization.

```
 %clear everything
clc
clf
clear all

%for nondimensionalization
kin = 0.06286;      %kinetic energy constant.
tstar = 0.00006772; %to convert from tau. tau * tstar = real t

%~~~~~~~~~~~~~~~Initialize Space~~~~~~~~~~~~~~~~~~~~~~~

Lx=100;                         %length of x
Nx=9000;                        %number of x data points
dx=2* Lx/Nx;
x=(-Lx:dx:Lx-2*Lx/Nx);          % x coordinate
kx=pi*[0:Nx/2 -Nx/2+1:-1]/(Lx);% wave vector
k2xm=kx.^2;                     %wave vector squared

%~~~~~~~~~~~~~Initialize Time~~~~~~~~~~~~~~~~~~~~~~~~~~
tf=1;                       %total time
dt=0.001;                   %time step
```

```
Nt=tf/dt;                 % number of time slices

tfExpan=25;               %so the expansion can be different
dtExpan=0.001;            %for the imaginary time expansion
NtExpan=tfExpan/dtExpan;

%%%~~~~~~~~~~~~~~~~~~~~~~~~Setting up Potential~~~~~~~~~
V0= 443.35;               %amplitude of softwall exponential term
Natoms = 2400;            %number of atoms
G= Natoms * 0.000277139;  %interaction term
Vwall = 2*10^9;           %height of wall x<0

%Potential itself
V= x + V0*exp(-x);
    V(x<=0) = Vwall;

    %~~~~~~~~~~~~~~~~~original guess~~~~~~~~~~~~
eps = 10000;
u=(1/sqrt(pi*eps))*exp((-.5/eps)*((x-0).^2)) ;

   %~~~~~~~~~~~~initializing stuff solving loop~~~~~~~~~~~~
pot=1; E=0; Mu=0; Ur=0; T=0; m=1; mm=1; n=0;
fracfun=0; %used for frac of remaining atoms
frac=0; %this is the fraction remaining
tauExpan=0;

 display('First Loop in Imaginary Time')
% In first for loop we calculated static wavefunction
% which we will use in next while loop as initial condition
% to determine time of flight
  while mm<Nt
    v=fft(u);
    vna=exp(-0.25*kin*dt.*(k2xm)).*v;
    una=ifft(vna);
    pot1=V+G*(abs(una)).^2;
    unb=exp(-dt*pot1).*una;
    vnb=fft(unb);
    v=exp(-0.25*kin*dt.*(k2xm)).*vnb;
    u=ifft(v);
```

```
    dx=2*Lx/Nx;
    intv=sum(u(:).^2)*dx;
    u=(u)./sqrt(intv);%phi function
    u1=u;
    u2=u;




     if(mod(mm-1,10)==0) %Plot solutions for each time interval
         figure(1)
         clf;

set(0,'defaulttextinterpreter','latex','DefaultAxesFontSize',20)
     % h=plot(x,phis,'r',x, phi,'b',x,abs(u).^2,'g','LineWidth',2);
     % x,abs(phis).^2,'r',
    h=plot(x,abs(u2).^2,'g','LineWidth',2);
       xlabel('$z$')
       ylabel('$\tilde{\Psi}(\tilde{z})$')
      axis([-Lx,Lx,-0, 1.1*max(u2.^2)])

        camlight right; lighting phong
        drawnow;

     end


      dk=dx;
    Kn=sum(k2xm.*fft(u1).^2)*dk/(2*Nx);
    E1=V.*abs(u1).^2+(G/2)*abs(u1).^4;
    E2=sum(E1)*dx;
    E(mm)=Kn+E2;%total energy

     TT(mm)=mm;




    mm=mm+1;
  end
```

```
maxy =  1.1*max(abs(u2).^2); %for scaling


%real time loop
display('Starting Real Time')

%potential
%pot1=x+G*(abs(una)).^2;  %do we need G???
  pot1=x;   %no G


while m<NtExpan


    %V=0; % Only for Time of flight calculation

    v=fft(u);
    vna=exp(-0.25*1i*kin*dtExpan.*(k2xm)).*v;
    una=ifft(vna);
    %pot1=x+G*(abs(una)).^2;
    unb=exp(-1i*dtExpan*pot1).*una;
    vnb=fft(unb);
    v=exp(-0.25*1i*kin*dtExpan.*(k2xm)).*vnb;
    u=ifft(v);
    dx=2*Lx/Nx;
    intv=sum(abs(u(:)).^2)*dx;
    u=(u)./sqrt(intv);
    u1=u;


    %for remaining frac
    fracfun = u;
    fracfun(x<=0) = 0;

    %integration of positive part
    frac(m)=sum(abs(fracfun(:)).^2)*dx;
```

```
    if(mod(m-1,10)==0) %Plot solutions for each time interval
    figure(2); clf;
    h=plot(x,abs(u1).^2,'g','LineWidth',2);

      xlabel('$z$')
       ylabel('$\tilde{\Psi}(\tilde{z})$')
 axis([-Lx,Lx,-0, maxy])

        camlight right; lighting phong
        drawnow;
    end

      dk=dx;
    MKn=sum(k2xm.*fft(abs(u1)).^2)*dk/(2*Nx);
    ME1=sum(V.*abs(u1).^2+(G)*abs(u1).^4)*dx;
       Mu(m)=MKn+ME1;


   %Double check below is width ie stand dev
   width(m)=sqrt(sum(x(:).^2.*abs(u1(:)).^2)*dx-(sum(x(:).*abs(u1(:)).^2)*dx).^2); %w

   %mean pos
   meanpos(m) = abs(sum( u(:).*x(:).*u(:) )*dx);

   %tau
   tauExpan(m) = m*tfExpan/NtExpan;


   m=m+1;


end


% fraction remaining
figure(6);

 scatter(tauExpan,frac,15,'MarkerEdgeColor','c',...
             'MarkerFaceColor','k',...
```

```
            'LineWidth',1.5)
           box on
          xlabel('$\tau$')
       ylabel('$Fraction Remaining$')
       title('Fraction of Atoms Remaining')
       axis([0,tfExpan,-0, 1.1])


  tReal = 10^(3)* tstar * tfExpan;   %convert max to ms
  tExpan = 10^(3)* tstar* tauExpan; %convert to ms
  % fraction remaining in real time
figure(7);

 scatter(tExpan,frac,15,'MarkerEdgeColor','c',...
             'MarkerFaceColor','k',...
            'LineWidth',1.5)
           box on
          xlabel('t in ms')
       ylabel('Fraction of Atoms Remaining')
       title('Real Time')
       axis([0,1.5,-0, 1.1])



name1 = sprintf('fraction.dat');
dlmwrite(name1,frac,'delimiter','\t')

name2 = sprintf('widthTOF.dat');
dlmwrite(name2,width,'delimiter','\t')

name3 = sprintf('meanposTOF.dat');
dlmwrite(name3,meanpos,'delimiter','\t')

dlmwrite('tau.dat',tauExpan,'delimiter','\t')
```

Bibliography

[1] M. H. Anderson, J. R. Ensher, M. R. Matthews, C. E. Wieman, and E. A. Cornell. Observation of bose-einstein condensation in a dilute atomic vapor. *Science*, 269 (5221):pp. 198–201, 1995. ISSN 00368075. URL http://www.jstor.org/stable/2888436.

[2] Franco Dalfovo, Stefano Giorgini, Lev Pitaevskii, and Sandro Stringari. Theory of bose-einstein condensation in trapped gases. *Rev. Mod. Phys.*, 71:463–512, Apr 1999. doi: 10.1103/RevModPhys.71.463. URL http://link.aps.org/doi/10.1103/RevModPhys.71.463.

[3] K. Davis, M. Mewes, M. Andrews, N. van Druten, D. Durfee, D. Kurn, and W. Ketterle. Bose-einstein condensation in a gas of sodium atoms. *Phys. Rev. Lett.*, 75:3969–3973, Nov 1995. doi: 10.1103/PhysRevLett.75.3969. URL http://link.aps.org/doi/10.1103/PhysRevLett.75.3969.

[4] C. Bradley, C. Sackett, J. Tollett, and R. Hulet. Evidence of bose-einstein condensation in an atomic gas with attractive interactions. *Phys. Rev. Lett.*, 75:1687–1690, Aug 1995. doi: 10.1103/PhysRevLett.75.1687. URL http://link.aps.org/doi/10.1103/PhysRevLett.75.1687.

[5] Nobelprize.org. The 2001 nobel prize in physics - advanced information. URL http://www.nobelprize.org/nobel_prizes/physics/laureates/2001/advanced.html.

[6] S. N. Bose. Plancks gesetz und lichtquantenhypothese. *Zeitschrift für Physik*, 1924.

[7] A. Einstein. Quantentheorie des einatomigen idealen Gases. *Sitzungsber. Kgl. Preuss. Akad. Wiss.*, 1924, 1924.

[8] D. Rychtarik, B. Engeser, H.-C. Nägerl, and R. Grimm. Two-dimensional bose-einstein condensate in an optical surface trap. *Phys. Rev. Lett.*, 92:173003, Apr 2004. doi: 10.1103/PhysRevLett.92.173003. URL http://link.aps.org/doi/10.1103/PhysRevLett.92.173003.

[9] Richard J. Cook and Richard K. Hill. An electromagnetic mirror for neutral atoms. *Optics Communications*, 43(4):258 – 260, 1982. ISSN 0030-4018. doi: http://dx.doi.org/10.1016/0030-4018(82)90392-3. URL http://www.sciencedirect.com/science/article/pii/0030401882903923.

[10] Harold J. Metcalf and Peter van der Straten. *Laser Cooling and Trapping*. Springer-Verlag, New York, 1999. ISBN 0387987282.

[11] Daniel Schroeder. *An introduction to thermal physics*. Addison Wesley, San Francisco, CA, 2000. ISBN 0201380277.

[12] Carl Wieman, Gwenn Flowers, and Sarah Gilbert. Inexpensive laser cooling and trapping experiment for undergraduate laboratories. *American Journal of Physics*, 63(4):317–330, 1995. doi: http://dx.doi.org/10.1119/1.18072. URL http://scitation.aip.org/content/aapt/journal/ajp/63/4/10.1119/1.18072.

[13] Eric Dodds. Progress toward bec through optimization and measurement of a compressed magneto-optical trap. Master's thesis, Pomona College, 2012.

[14] M. D. Barrett, J. A. Sauer, and M. S. Chapman. All-optical formation of an atomic bose-einstein condensate. *Phys. Rev. Lett.*, 87:010404, Jun 2001. doi: 10.1103/PhysRevLett.87.010404. URL http://link.aps.org/doi/10.1103/PhysRevLett.87.010404.

[15] Wolfgang Petrich, Michael H. Anderson, Jason R. Ensher, and Eric A. Cornell. Stable, tightly confining magnetic trap for evaporative cooling of neutral atoms. *Phys. Rev. Lett.*, 74:3352–3355, Apr 1995. doi: 10.1103/PhysRevLett.74.3352. URL http://link.aps.org/doi/10.1103/PhysRevLett.74.3352.

[16] M. Hammes, D. Rychtarik, V. Druzhinina, U. Moslener, I. Manek-Hönninger, and R. Grimm. Optical and evaporative cooling of caesium atoms in the gravito-optical surface trap. *Journal of Modern Optics*, 47(14-15):2755–2767, 2000. doi: 10.1080/09500340008232195. URL http://www.tandfonline.com/doi/abs/10.1080/09500340008232195.

[17] John Townsend. *A modern approach to quantum mechanics*. University Science Books, Sausalito, Calif, 2012. ISBN 978-1891389788.

[18] J. J. Sakurai. *Advanced quantum mechanics*. Addison-Wesley Pub. Co, Reading, Mass, 1967. ISBN 978-0201067101.

[19] Franz Schwabl. *Advanced quantum mechanics*. Springer, Berlin, 2008. ISBN 978-3540850618.

[20] R Carretero-González, D J Frantzeskakis, and P G Kevrekidis. Nonlinear waves in bose–einstein condensates: physical relevance and mathematical techniques. *Nonlinearity*, 21(7):R139, 2008. URL http://stacks.iop.org/0951-7715/21/i=7/a=R01.

[21] Anthony J. Leggett. Bose-einstein condensation in the alkali gases: Some fundamental concepts. *Rev. Mod. Phys.*, 73:307–356, Apr 2001. doi: 10.1103/RevModPhys.73.307. URL http://link.aps.org/doi/10.1103/RevModPhys.73.307.

[22] Yu. B. Ovchinnikov, I. Manek, and R. Grimm. Surface trap for cs atoms based on evanescent-wave cooling. *Phys. Rev. Lett.*, 79:2225–2228, Sep 1997. doi: 10.1103/PhysRevLett.79.2225. URL http://link.aps.org/doi/10.1103/PhysRevLett.79.2225.

[23] A. Muñoz Mateo and V. Delgado. Extension of the thomas-fermi approximation for trapped bose-einstein condensates with an arbitrary number of atoms. *Phys. Rev. A*, 74:065602, Dec 2006. doi: 10.1103/PhysRevA.74.065602. URL http://link.aps.org/doi/10.1103/PhysRevA.74.065602.

[24] R W Robinett. Image method solutions for free-particle wave packets in wedge geometries. *European Journal of Physics*, 27(2):281, 2006. URL http://stacks.iop.org/0143-0807/27/i=2/a=011.

[25] Juha Javanainen and Janne Ruostekoski. Symbolic calculation in development of algorithms: split-step methods for the gross–pitaevskii equation. *Journal of Physics A: Mathematical and General*, 39(12):L179, 2006. URL http://stacks.iop.org/0305-4470/39/i=12/a=L02.

[26] Julio Gea-Banacloche. A quantum bouncing ball. *American Journal of Physics*, 67(9):776–782, 1999. doi: http://dx.doi.org/10.1119/1.19124. URL http://scitation.aip.org/content/aapt/journal/ajp/67/9/10.1119/1.19124.